LEARNING GRAPH INVARIANCE BY HARNESSING SPURIOSITY

Anonymous authors
Paper under double-blind review

ABSTRACT

Recently, graph invariant learning has become the *de facto* approach to tackle the Out-of-Distribution (OOD) generalization failure in graph representation learning. They generally follow the framework of invariant risk minimization to capture the invariance of graph data from different environments. Despite some success, it remains unclear to what extent existing approaches have captured invariant features for OOD generalization on graphs. In this work, we find that representative OOD methods such as IRM and VRex, and their variants on graph invariant learning may have captured a limited set of invariant features. To tackle this challenge, we propose **LIRS**, a novel learning framework designed to **L**earn graph **I**nvariance by **R**emoving **S**purious features. Different from most existing approaches that *directly* learn the invariant features, LIRS takes an *indirect* approach by first learning the spurious features and then removing them from the ERM-learned features. We demonstrate that learning the invariant graph features in an *indirect* way enables the model to capture a more comprehensive set of invariant features, leading to better OOD generalization performance in novel environments. Notably, LIRS surpasses the second-best method by as much as 25.50% across all competitive baselines, underscoring its efficacy in OOD generalization.

1 INTRODUCTION

Graph representation learning with graph neural networks (GNNs) (Kipf & Welling, 2017; Xu et al., 2019; Veličković et al., 2017) has proven to be highly successful in tasks involving relational information (Qiu et al., 2018; Wu et al., 2022b; Yu et al., 2018; Zhang et al., 2022c). Despite their achievements, GNNs often assume that the training and test data share the same distribution. This assumption often does not hold in real-world applications (Hu et al., 2020; Huang et al., 2021; Ji et al., 2022; Koh et al., 2021) due to changes in the underlying data generation process, leading to distribution shifts. Such phenomenon can severely degrade the performance of GNN models, which presents a critical challenge for their deployment in practical scenarios (DeGrave et al., 2020).

To address the OOD generalization challenge, graph invariant learning has become the *de facto* approach. Inspired by the success of invariance principle (Arjovsky et al., 2020; Kreuzer et al., 2021), graph invariant learning aims to identify invariant subgraphs that are causally related with the targets (Yang et al., 2022; Li et al., 2022b; Liu et al., 2022; Zhuang et al., 2023; Chen et al., 2022; Li et al., 2022a). Typically, they follow the framework of Invariant Risk Minimization (IRM) (Arjovsky et al., 2020) or Variance-Risk Minimization (VRex) (Krueger et al., 2021), which aim to capture invariant features by learning an equipredictive classifier across different environments. Despite some success, many graph invariant learning methods only perform similarly compared to the traditional Empirical Risk Minimization (ERM) (Vapnik, 1995) in graph OOD benchmarks (Gui et al., 2022), it raises a critical yet overlooked question:

To what extent do the graph invariant learning algorithms capture the graph invariance?

In this work, we address this question by investigating two representative OOD algorithms, namely IRMv1 (Arjovsky et al., 2020) and VRex (Kreuzer et al., 2021), in graph-level OOD classification scenarios. These algorithms are widely used, and many graph invariance learning algorithms are based on their variants or extensions (Li et al., 2022b; Liu et al., 2022; Zhuang et al., 2023; Wu et al., 2022c). Surprisingly, we find that IRM, VRex and their variants on graph invariant learning

may only learn *a subset* of invariant features (Sec. 3). In contrast, the learning paradigm that learns invariant features *indirectly* by removing spurious features from the ERM-learned features may render learning a more comprehensive set of invariant features (Figure 1 and Sec. 3). Motivated by this observation, we propose a novel learning framework **LIRS**: **L**earning graph **I**nvariance by **R**emoving **S**puriosity. Different from most existing approaches that *directly* learn the invariant features, LIRS adopts the *indirect* learning paradigm. Specifically, LIRS first leverages the *biased infomax principle* (Def. 3) to effectively learn graph spuriosity (Theorem 4.1), then employees *class-conditioned cross entropy loss* to effectively learn graph invariance (Theorem 4.2). Extensive experiments on synthetic datasets demonstrate that LIRS is able to learn more invariant features compared to state-of-the-art graph invariant learning methods that adopt the direct invariant learning paradigm. Furthermore, LIRS shows superior OOD performance on real-world datasets with various types of distribution shifts, highlighting its effectiveness in learning graph invariant features. Our contributions can be summarized as follows:

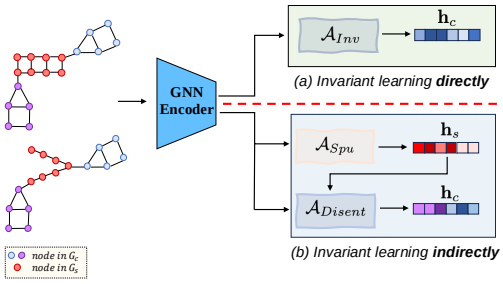

Figure 1: Illustration of the two graph invariant learning paradigms. Compared with the invariant learning methods $\mathcal{A}_{Inv}$ that adopt the direct learning paradigm, our proposed method first adopts a spuriosity learner $\mathcal{A}_{Spu}$ to learn spurious features, then learns invariant features by removing the spurious features using the feature disentanglement module $\mathcal{A}_{Disent}$.

- We reveal that learning invariant features *indirectly* i.e., by first learning and then removing spurious features, can be more effective in capturing invariant features than existing (graph) invariant learning algorithms that learn invariant features *directly*.
- We propose **LIRS**, a novel framework that adopts the indirect learning paradigm for learning invariant features, which consists of: a) The *biased infomax principle*, a contrastive learning algorithm that provably learns graph spuriosity; b) *class-conditioned cross-entropy loss*, a learning objective that effectively learns graph invariance by removing spurious features from ERM-learned features.
- Extensive experiments demonstrate that LIRS outperforms second-best baseline methods by up to 25.50% across 17 competitive baselines on both synthetic and real-world datasets with various distribution shifts.

2 PRELIMINARY

Notations. An undirected graph G with n nodes and m edges is denoted by $G := \{\mathcal{V}, \mathcal{E}\}$, where $\mathcal{V}$ is the node set and $\mathcal{E}$ is the edge set. G is also represented by the adjacency matrix $\mathbf{A}$ and the node feature matrix $\mathbf{X} \in \mathbb{R}^{n \times D}$ with D feature dimensions. We use G_c and G_s to denote invariant and spurious subgraph for graph G respectively, and $\mathbf{h}_c$ and $\mathbf{h}_s$ are invariant and spurious features in the latent space. $\widehat{\mathbf{h}}_i$ and $\widehat{\mathbf{h}}_G$ denote the estimated representations for node v_i and graph G respectively. Finally, we use $[K] := \{1, 2, \ldots, K\}$ to denote an index set, w to denote a scalar value, $\mathbf{w}$ to denote a vector, $\mathbf{W}$ to denote a matrix, W to denote a random variable, and $\mathcal{W}$ to denote a set. A more complete set of notations is presented in Appendix A.

Problem Definition. We focus on OOD generalization in graph classification in hidden environments. Given a set of graph datasets $\mathcal{D} = \{\mathcal{G}^e\}_{e \in \mathcal{E}_{\text{tr}} \subseteq \mathcal{E}_{\text{all}}}$, a GNN model f, denoted as $\rho \circ h$, comprises an encoder $h : \mathbb{G} \to \mathbb{R}^F$ that learns a representation $\mathbf{h}_G$ for each graph G, followed by a downstream classifier $\rho : \mathbb{R}^F \to \mathbb{Y}$ to predict the label $\widehat{Y}_G = \rho(\widehat{\mathbf{h}}_G)$. The objective of OOD generalization on graphs is to learn an optimal GNN model $f^*(\cdot) : \mathbb{G} \to \mathbb{Y}$ using data from training environments $\mathcal{D}_{\text{tr}} = \{\mathcal{G}^e\}_{e \in \mathcal{E}_{\text{tr}}}$ that effectively generalizes across all (unseen) environments: $f^*(\cdot) = \arg\min_f \sup_{e \in \mathcal{E}_{\text{all}}} \mathcal{R}(f \mid e)$, where $\mathcal{R}(f \mid e) = \mathbb{E}^e_{G,Y}[l(f(G), Y)]$ is the risk of the predictor f on the environment e, and $l(\cdot, \cdot) : \mathbb{Y} \times \mathbb{Y} \to \mathbb{R}_+$ denotes a loss function.

Assumption 1. (**Stable and predictive subgraphs**) Given a graph $G \in \mathcal{D}$, there exists a set of stable (causal) substructure patterns $\mathcal{G}_c$ for every class label $Y = y$, satisfying: a) $\forall e, e' \in \mathcal{E}_{tr}, G_c \in$

$\mathcal{G}_c, \mathbb{P}^e(Y \mid G_c) = \mathbb{P}^{e'}(Y \mid G_c)$; and b) The target Y can be expressed as $Y = f^*(G_c) + \epsilon$, where $\epsilon \perp\!\!\!\perp G$ represents random noise, and $\perp\!\!\!\perp$ indicates statistical independence.

Assumption 1 posits that one or more substructure patterns in $\mathcal{G}_c$ are not only stably associated with the target label Y across different environments but also possess sufficient predictive power to accurately determine Y. This assumption is well-aligned with real-world scenarios. For instance, in the GOODHIV dataset (Gui et al., 2022; Hu et al., 2020; Wu et al., 2018), a molecule's ability to inhibit HIV may depend on the presence of several functional groups interacting with various parts of the virus. Moreover, recent study also provides empirical evidence for graph applications, suggesting that multiple substructures remain stable and predictive of the targets (see Appendix E.2 in Bui et al. (2024)), thereby supporting the validity of Assumption 1. Therefore, when the OOD algorithms are able to learn a broader set of invariant substructures (features), they will generalize more effectively across different environments.

3 Why Learning Invariant Features Indirectly?

In this section, we motivate our study by addressing the question: *Why might learning invariant features indirectly be more effective than learning them directly?* We begin by presenting an intuitive hypothesis related to our research question, followed by an empirical study on synthetic datasets to support this hypothesis. Consider a dataset $\mathcal{D}$ where each sample $G^{(i)}$ comprises invariant features $\{\mathbf{h}_{c,j}^{(i)}\}_{j=1}^{n_c}$ and spurious features $\{\mathbf{h}_{s,j}^{(i)}\}_{j=1}^{n_s}$, with n_c and n_s denoting the number of invariant and spurious features respectively. Any subset of the invariant features $\{\mathbf{h}_{c,j}^{(i)}\}_{j=1}^{n_c}$ maintains stable relationships with Y, consequently OOD objectives that aim to directly learn invariant features (e.g., IRMv1 and VREx) may only capture a subset of these invariant features if a subset of invariant features can already achieve accurate predictions in the training set. In contrast, an OOD objective that seeks to remove the spurious features $\{\mathbf{h}_{s,j}^{(i)}\}_{j=1}^{n_s}$ from the ERM-learned features may result in learning a more complete set of invariant features from $\{\mathbf{h}_{c,j}^{(i)}\}_{j=1}^{n_c}$, thus facilitating OOD generalization in unseen environments.

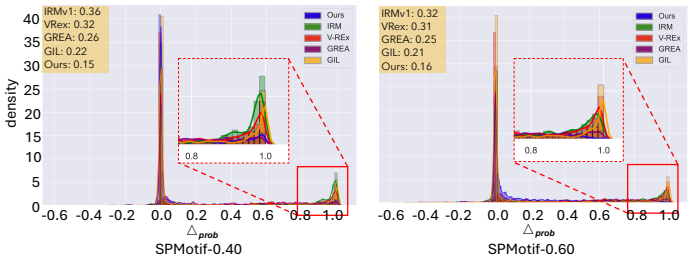

Figure 2: Comparison of the distribution $\mathbb{P}_{\Delta_{prob}}$ across different OOD algorithms.

Empirical Study. To validate our hypothesis that learning invariant features by removing spurious features may facilitate learning more invariant features, we perform experiments using a variant of SPMotif datasets (Wu et al., 2022c; Ying et al., 2019). Specifically, for each sample three invariant subgraphs are attached to the base spurious subgraph in the training and validation sets. In the test dataset, we perform model inference and record the estimated probability for *correctly predicted samples*, denoted as $\hat{y}_j^{(i)}$. Subsequently, we randomly removed two invariant subgraphs from these samples and compute the new estimated probability score, denoted as $\tilde{y}_j^{(i)}$. We then fit the distribution $\mathbb{P}_{\Delta_{prob}}$ using Kernel Density Estimation (KDE) (Terrell & Scott, 1992), based on the changes in probability $\Delta_{prob} := \hat{y}_j^{(i)} - \tilde{y}_j^{(i)}, \ \forall i, j$, as illustrated in Figure 2. If the encoder $h(\cdot)$ can indeed learn all invariant features in the test set, then removing two invariant subgraphs should not change $\hat{y}_j^{(i)}$. Therefore, the closer $\mathbb{P}_{\Delta_{prob}}$ is to 0, the more it indicates that the encoder has learned the full set of invariant features. In addition to the density function of Δ_{prob}, we also calculate the Wasserstein distance of each algorithm to a null distribution, where the probability mass is entirely centered at 0. As demonstrated in Figure 2, IRMv1 (Arjovsky et al., 2020) and VRex (Krueger et al., 2021) exhibit significant changes in Δ_{prob}, implying that for some samples, IRMv1 and VRex learn only a subset of the invariant patterns. GIL (Li et al., 2022b) and GREA (Liu et al., 2022) are two variants of VRex and IRM that learn invariant features directly by performing environment inference and environment augmentation respectively. As shown in Figure 2, the Wasserstein distances for GIL (Li et al., 2022b) and GREA (Liu et al., 2022) are also greater than that of our proposed

method. This highlights the advantages of the learning paradigm that indirectly learns invariant features by first learning and then removing spuriosity. However, one may raise concerns that while learning invariant features by first removing spurious features may indeed lead to capturing a more complete set of invariant features for the correctly predicted samples, it may also introduce spurious patterns if the spurious features are not effectively removed, which could render such a learning paradigm suboptimal in practice. To address this concern, we report test accuracy under varying strengths of spurious correlations, following previous experiments. As the strength of the spurious correlation increases, it becomes more challenging to eliminate the spurious features. From Figure 3, we have three observations: a) Our method consistently achieves superior OOD performance across different correlation strengths; b) Our method is less sensitive to the increased spurious correlations compared to other representative OOD methods, which is evident by the flatter curve in Figure 3; c) The higher test accuracy, combined with the distribution of probability changes from the previous experiment, suggests that our method enables a larger number of test samples to learn a more complete set of invariant features. Based on these observations and analysis, we conclude that indirectly learning invariant features is more effective than learning them directly.

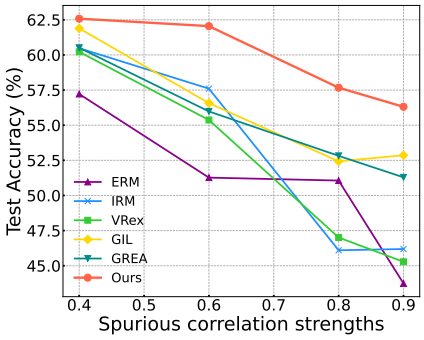

Figure 3: Test accuracy under varying spurious correlation strengths of the variant of SPMtoif datasets.

4 METHODOLOGY

Motivated by the observations in Sec. 3, we now introduce our proposed **LIRS** framework, which learns invariant features on graphs *indirectly*.

4.1 LEARNING GRAPH SPURIOSITY VIA BIASED INFOMAX

The first step of learning invariant features in the LIRS framework is to effectively learn graph spuriosity. In this section, we first propose a variant of the infomax principle (Hjelm et al., 2019; Veličković et al., 2019; Linsker, 1988), namely *biased infomax*, which encourages spuriosity learning by suppressing invariant signals. We then present a more practical version of biased infomax, suitable for the real-world datasets. We first formally define *spuriosity learning* in below:

Definition 1. (*Spuriosity Learning*) Assuming each data instance $G^{(i)}$ in a dataset $\mathcal{D}$ is composed of two parts $\mathbf{h}_c^{(i)}$ and $\mathbf{h}_s^{(i)}$, an algorithm $\mathcal{A}$ is said to be a spuriosity learner if $\mathbf{h}_s^{(i)} = \mathcal{A}(G^{(i)}),\ \forall i$, i.e., $\mathcal{A}$ learns only the spurious features for all instances in $\mathcal{D}$.

One such algorithm to encourage spuriosity learning is the *global-local infomax principle* (Hjelm et al., 2019; Veličković et al., 2019; Linsker, 1988), which maximizes the mutual information (MI) between global representation and local node representations, as defined in the following:

Definition 2. (*The Infomax Principle*) The infomax principle optimizes the following optimization objective in Eqn. 1 w.r.t the GNN encoder $h_\theta(\cdot)$.

$$\max_{\theta}\ \mathbb{E}_{G\sim\mathcal{G}} \frac{1}{|G|} \sum_{v_i \in G} I\left(\widehat{\mathbf{h}}_i, \widehat{\mathbf{h}}_G\right),\ s.t.\ \widehat{\mathbf{h}}_i = h_\theta(G), \widehat{\mathbf{h}}_G = READOUT(\widehat{\mathbf{h}}_i). \tag{1}$$

The encoder $h_\theta(\cdot)$ will primarily learn spurious features (Yao et al., 2024). However, it will still be constrained by $|G_c|$, the size of the invariant subgraph. As $|G_c|$ increases, the learned global representation $\widehat{\mathbf{h}}_G$ will increasingly capture invariant representations (Yao et al., 2024). To mitigate this constraint and further facilitate spuriosity learning, we propose the *biased infomax principle*.

Definition 3. (*The Biased Infomax Principle*) The biased infomax principle optimizes the following optimization objective in Eqn. 2 w.r.t the GNN encoder $h_\theta(\cdot)$.

$$\max_{\theta} \ \mathbb{E}_{G\sim\mathcal{G}} \frac{1}{|G|}\left(\sum_{v_i\in G_s} I\left(\widehat{\mathbf{h}}_i,\widehat{\mathbf{h}}_G\right) - \sum_{v_i\in G_c} I\left(\widehat{\mathbf{h}}_i,\widehat{\mathbf{h}}_G\right)\right), \ \text{s.t. } \widehat{\mathbf{h}}_i = h_\theta(G), \ \widehat{\mathbf{h}}_G = \text{READOUT}(\widehat{\mathbf{h}}_i). \tag{2}$$

By maximizing MI across nodes $v_i \in G_s$ and minimizing MI across nodes $v_i \in G_c$, the biased infomax principle yields an encoder $h_{\theta^*}(\cdot)$ that encourages the learning of spurious patterns while suppressing invariant ones. Formally, we can demonstrate that the biased infomax principle achieves spuriosity learning.

Theorem 4.1. *Given that the invariant subgraph G_c contains invariant patterns that are causally related to the target labels, and G_s contains only spurious patterns, the biased infomax principle achieves spuriosity learning, i.e., the encoder $h_{\theta^*}(\cdot)$ learns solely the spurious features for each data sample G in $\mathcal{D}$.*

To achieve invariant learning by removing spuriosity, it is crucial to effectively learn the spurious features first. Theorem 4.1 demonstrates that the biased infomax principle can learn graph spuriosity more effectively the vanilla infomax, as defined in Def. 2. However, in real-world scenarios, G_c is often unobservable, which hinders the practicality of the biased infomax principle. To make the proposed algorithm more practical, we propose an instance-level adaptive biased infomax, which incorporates a GNN explainer to identify the important nodes first, and then performs instance-wise counterfactual inference to determine whether the selected nodes should be biased or not.

Instance-level adaptive biased infomax. At first glance, the biased infomax principle appears impractical due to the necessity of knowing G_c and G_s. To address this limitation, we employ an approximation algorithm to identify $\widehat{G}_c$, which serves as an estimate for G_c. Subsequently, we treat nodes $v_i \in \widehat{G}_c$ to realize the biased infomax principle. In practice, we utilize GSAT (Miao et al., 2022), a GNN explainer $e(\cdot)$ that is robust under distribution shifts, to identify $\widehat{G}_c$ and $\widehat{G}_s = G \setminus \widehat{G}_c$. Nevertheless, the approximation error may inadvertently bias the algorithm by amplifying invariant signals and suppressing spurious ones, as demonstrated in the following proposition.

Proposition 1. *Given an error rate $p\%$ in the approximation algorithm for G_c, i.e., $\widehat{G}_c$ contains $1-p\%$ nodes from G_c and $p\%$ nodes from G_s, let the learning objectives for the biased infomax with the ground-truth subgraphs G_c and G_s and with the approximated subgraphs $\widehat{G}_c$ and $\widehat{G}_s$ be denoted as $\mathcal{L}(\theta^*;\mathcal{D})$ and $\mathcal{L}(\theta';\mathcal{D})$ respectively. The difference between $\mathcal{L}(\theta^*;\mathcal{D})$ and $\mathcal{L}(\theta';\mathcal{D})$ can be expressed as:*

$$\mathbb{E}_{G\sim\mathcal{G}}\left[\frac{2}{|G|}\left(\sum_{v_i\in pG_s} I\left(\widehat{\mathbf{h}}_i;\widehat{\mathbf{h}}_G\right) - \sum_{v_i\in pG_c} I\left(\widehat{\mathbf{h}}_i;\widehat{\mathbf{h}}_G\right)\right)\right].$$

Here pG denotes $p\%$ nodes in graph G. When $\widehat{\mathbf{h}}_G$ learns primarily spurious features, $I\left(\widehat{\mathbf{h}}_i;\widehat{\mathbf{h}}_G\right) > I\left(\widehat{\mathbf{h}}_j;\widehat{\mathbf{h}}_G\right), \forall v_i \in G_s, v_j \in G_c$, then Prop. 1 implies that as $p\%$ increases, the gap between the ground-truth learning objective and the learning objective with approximation will also increase, thus leading to inaccurate graph representations. To reduce the approximation error and mitigate this issue, we conduct *counterfactual inference* for a graph G by evaluating the changes in predicted probability with and without $\widehat{G}_c$ derived from the GNN explainer. Assuming $\widehat{G}_c = e(G,Y)$ closely approximates the ground-truth G_c, the removal of $\widehat{G}_c$ should result in a significant change in the predicted probability score. Under this condition, for graph G, we bias $v_i \in \widehat{G}_c$. Otherwise, we employ vanilla infomax without the bias operation. Specifically, we use a pre-defined threshold τ. For each graph data instance $G^{(i)}$ with target label j, let $\widehat{y}_j^{(i)}$ and $\tilde{y}_j^{(i)}$ denote the predicted probability scores before and after the removal of $\widehat{G}_c$, respectively. We then bias the infomax for graph $G^{(i)}$ if $\widehat{y}_j^{(i)} - \tilde{y}_j^{(i)} > \tau$ using Eqn. 2; otherwise, we use Eqn. 1 to learn the graph representation.

4.2 Learning Graph Invariance via Class-conditioned Cross-entropy Loss

Class-conditioned cross-entropy loss. So far we have obtained the spurious graph representations $\mathbf{h}_s$ for every instance G in the dataset. Next we consider how to learn graph invariance by re-

moving the spurious features from ERM-learned representations. To solve this challenge, previous study (Yao et al., 2024) takes spurious features $\mathbf{h}_s$ and target label Y as inputs to train a linear classifier using cross-entropy loss to obtain the logits, which capture spurious correlation for each sample G, and use these (spurious) logits for subsequent spurious feature removing. Although the input only contains spurious features, we argue that: *The logits generated may be inaccurate to capture the spurious correlation strengths due to the overlapping of spurious patterns across different classes.* To see this, we propose Prop. 2 to demonstrate this issue:

Proposition 2. *Given a linear regression model with parameters $\{\theta_1, \theta_2\}$ and spurious features $\{x_1, x_2\}$, the correlation strength for feature x_1 is p and for x_2 is $1-p$ when $Y=0$. Similarly, the correlation strength for feature x_1 is q and for x_2 is $1-q$ when $Y=1$. Assuming the spurious features x_1 and x_2 can each take values in $\{0,1\}$, we obtain the following parameter estimates using Mean Squared Error (MSE) loss: $\theta_1 = \frac{q}{p+q}, \theta_2 = \frac{1-q}{2-p-q}$.*

Prop. 2 demonstrates the issue brought by the interference of overlapping spurious features across different classes. For instance, when $p = q$, $\theta_1 = \theta_2 = \frac{1}{2}$, the generated logits fail to distinguish different spurious patterns. To mitigate this issue, we propose *class-conditioned cross-entropy loss*. Specifically, we first perform clustering within each class based on the spurious features $\{\mathbf{h}_s^{(i)}\}_{i=1}^n$. The resulted clusters will reflect different spurious patterns and environments accurately given the spurious features learned by the biased infomax objective. However, employing hard labels can result in a loss of information regarding the relative positions of samples within a cluster. To address this, we refit a linear classifier using the cluster labels as targets. This approach ensures that samples near the cluster boundaries exhibit higher entropy in their spurious logits, thereby preserving the information about their position within the cluster. Given the estimated spurious logits $\mathbf{s}^{(i)} \in \mathbb{R}^K$ with K clusters in each class, we propose the following learning objective for spurious feature removing:

$$\mathcal{L}_{\text{inv}} := \mathbb{E}_{y\sim\mathcal{Y}}\, \mathbb{E}_{G^{(i)}|Y=y}\ -\sum_{j=1}^{K} w^{(i)}\mathbf{s}_j^{(i)} \log\left(\sigma(\widehat{\mathbf{s}}_j^{(i)})\right),\ s.t., \widehat{\mathbf{s}}^{(i)} = \rho'(\widehat{\mathbf{h}}_G^{(i)}) \in \mathbb{R}^K. \tag{3}$$

Here, $\sigma(\cdot)$ denotes the softmax function, $\rho'(\cdot) : \mathbb{R}^F \to \mathbb{R}^C$ represents the clustering classification head, which takes $\widehat{\mathbf{h}}_G$ from the GNN encoder $h(\cdot)$ as input. The reweighting coefficient for each sample $G^{(i)}$ is denoted as $w^{(i)}$, which adjusts the weight for samples from the majority group by reducing it and increases the weight for samples from the minority group. The generalized cross-entropy (GCE) method (Zhang & Sabuncu, 2018) is employed to calculate $w^{(i)}$, i.e., $w^{(i)} = \frac{1-\left(\mathbf{s}_j^{(i)}\right)^\gamma}{\gamma}$, where j is the ground-truth clustering label for sample $G^{(i)}$, and γ is a hyperparameter. Finally, The loss objective for feature disentanglement is:

$$\mathcal{L} = \mathcal{L}_{GT} + \lambda\mathcal{L}_{inv}, \tag{4}$$

where $\mathcal{L}_{GT}$ denotes the ERM loss. $\mathcal{L}_{inv}$, serving as a regularization term, will guide the learning process to learn invariant features by removing spurious features from the ERM-learned features. Formally, we present the following theorem.

Theorem 4.2. *There exists a suitable γ and clustering number K, such that minimizing the loss objective $\mathcal{L} = \mathcal{L}_{GT} + \lambda\mathcal{L}_{inv}$ will lead to the optimal encoder $h^*(\cdot)$ which elicits invariant features for any graph G, i.e., $\widehat{\mathbf{h}}_G = h^*(G) = \mathbf{h}_c$.*

The proof is included in Appendix D. In the proof of Theorem 4.2, we show that $\mathcal{L}_{inv}$ will guide the ERM-learned features to focus on invariant features by removing or unlearning the spurious ones. More concretely, given ERM learns both invariant and spurious features (Kirichenko et al., 2023; Chen et al., 2023b), i.e., $\widehat{\mathbf{h}}_G = \kappa(\mathbf{h}_c, \mathbf{h}_s)$, where $\kappa(\cdot)$ is a functional mapping to graph representation $\widehat{\mathbf{h}}_G$ given a set of invariant features $\mathbf{h}_c$ and a set of spurious features $\mathbf{h}_s$, $\mathcal{L}_{inv}$ regularizes the learning process to optimize $\kappa^*(\cdot)$ such that $\widehat{\mathbf{h}}_G$ contains only $\mathbf{h}_c$. While previous OOD methods achieve a similar goal (to learn only invariant features), our approach differs by first learning the spurious features and then leveraging them to identify the causal features from the ERM-learned features, a process we refer to as *spurious feature removing or unlearning*.

Table 1: Performance on synthetic and real-world datasets. Numbers in **bold** indicate the best performance, while the underlined numbers indicate the second best performance.

Method	GOOD-Motif		GOOD-HIV		OGBG-Molbace		OGBG-Molbbbp	
	base	size	scaffold	size	scaffold	size	scaffold	size
ERM	68.66±4.25	51.74±2.88	69.58±2.51	59.94±2.37	75.11±3.03	83.60±3.47	68.10±1.68	78.29±3.76
IRM	70.65±4.17	51.41±3.78	67.97±1.84	59.00±2.92	75.47±2.22	83.12±2.58	67.22±1.15	77.56±2.48
GroupDRO	68.24±8.92	51.95±5.86	70.64±2.57	58.98±2.16	-	-	66.47±2.39	79.27±2.43
VREx	71.47±6.69	52.67±5.54	70.77±2.84	58.53±2.88	72.81±4.29	82.55±2.51	68.74±1.03	78.76±2.37
RSC	46.12±3.76	51.70±5.47	69.16±3.23	61.17±0.74	74.59±3.65	84.34±2.65	69.01±2.84	78.07±3.89
DiverseModel	54.24±8.22	41.01±1.98	69.17±3.62	61.59±2.23	73.48±3.56	79.40±1.70	68.04±3.27	77.62±1.90
DropEdge	45.08±4.46	45.63±4.61	70.78±1.38	58.53±1.26	70.81±2.12	76.39±2.29	66.49±1.55	78.32±3.44
FLAG	61.12±5.39	51.66±4.14	68.45±2.30	60.59±2.95	80.37±1.58	84.72±0.88	67.69±2.36	79.26±2.26
LiSA	54.59±4.81	53.46±3.41	70.38±1.45	52.36±3.73	78.05±5.01	83.92±2.52	68.11±0.52	78.62±3.74
DIR	62.07±8.75	52.27±4.56	68.07±2.29	58.08±2.31	75.49±2.80	77.42±7.43	66.86±2.25	76.40±4.43
DisC	51.08±3.08	50.39±1.15	68.07±1.75	58.76±0.91	57.78±3.60	71.13±8.86	67.12±2.11	56.59±10.09
CAL	65.63±4.29	51.18±5.60	67.37±3.61	57.95±2.24	76.29±1.60	79.68±4.06	68.06±2.60	79.50±4.81
GREA	56.74±9.23	54.13±10.02	67.79±2.56	60.71±2.20	77.16±1.37	83.15±9.07	69.72±1.66	77.34±3.52
GSAT	62.80±11.41	53.20±8.35	68.66±1.35	58.06±1.98	72.32±5.66	82.45±2.73	66.78±1.45	75.63±3.83
CIGA	66.43±11.31	49.14±8.34	69.40±2.39	59.55±2.56	76.44±1.72	83.95±2.75	64.92±2.09	65.98±3.31
AIA	73.64±5.15	55.85±7.98	71.15±1.81	61.64±3.37	79.42±2.01	85.11±0.74	70.79±1.53	81.03±5.15
OOD-GCL	56.46±4.61	60.23±8.49	70.85±2.07	58.48±2.94	75.96±2.21	85.34±1.77	67.28±3.09	78.11±3.32
EQuAD	67.11±10.11	59.72±3.69	72.24±0.64	64.19±0.56	79.15±2.32	86.41±5.63	70.22±2.36	80.82±5.28
LIRS	**75.51±2.19**	**74.95±7.69**	**72.82±1.61**	**66.64±1.44**	**81.91±1.98**	**88.77±1.64**	**71.04±0.76**	**82.19±1.57**

5 EXPERIMENTS

In this section, we perform empirical study on both synthetic and real-world datasets. More details about the datasets and experiment setup are included in Appendix H.

5.1 EXPERIMENTAL SETUP

Datasets. We adopt GOODMotif and GOODHIV datasets (Gui et al., 2022), OGBG-Molbace and OGBG-Molbbbp datasets (Hu et al., 2020; Wu et al., 2018) to comprehensively evaluate the OOD generalization performance of our proposed framework. For GOODMotif datasets, we adopt base shift and size shift, for OGBG datasets, in addition to scaffold shift, we also create size shift, following previous studies (Gui et al., 2022; Sui et al., 2023). More details on the datasets used in our work are included in Appendix H.

Baselines. Besides ERM (Vapnik, 1995), we compare our method against three lines of OOD baselines: (1) OOD algorithms on Euclidean data, including IRM (Arjovsky et al., 2020), VREx (Krueger et al., 2021), and GroupDRO (Sagawa et al., 2019); (2) Diverse feature learning methods, including RSC (Huang et al., 2020), and DiverseModel (Teney et al., 2022). (3) graph-specific OOD and data augmentation algorithms without requiring environment labels, including DIR (Wu et al., 2022c), GSAT (Miao et al., 2022), GREA (Liu et al., 2022), DisC (Fan et al., 2022), CIGA (Chen et al., 2022), AIA (Sui et al., 2023), OOD-GCL (Li et al., 2024a), EQuAD (Yao et al., 2024), DropEdge (Rong et al., 2019), FLAG (Kong et al., 2022), and LiSA (Yu et al., 2023). Details of the baselines and their implementation are provided in Appendix H.

Evaluation. We report the ROC-AUC score for GOOD-HIV, OGBG-Molbbbp, and OGBG-Molbace datasets, where the tasks are binary classification. For GOOD-Motif and SPMotif datasets, we use accuracy as the evaluation metric. We run experiments 4 times with different random seeds, select models based on the validation performance, and report the mean and standard deviations on the test set.

5.2 EXPERIMENTAL RESULTS

In this section, we report the main results on both synthetic and real-world datasets.

Synthetic datasets. For the GOOD-Motif datasets, LIRS demonstrates its superiority by outperforming the second-best method by 12.51% and 25.50% in the base and size split respectively. This substantial margin highlights the effectiveness of LIRS in capturing domain-invariant features across different types of distribution shifts. Although EQuAD adopts a similar learning paradigm

by attempting to remove spurious features, LIRS outperforms it by 25.50% in the size split of the GOOD-Motif datasets. The underlying reason for this performance gap is that in the training set of GOOD-Motif, the spurious subgraph G_s occupies a significant portion of the graph. The infomax principle adopted in EQuAD can inadvertently affect the learning of spurious features and hinder the subsequent invariant learning process. In contrast, LIRS adopts biased infomax, which facilitates the suppression of invariant signals, thereby allowing it to learn spurious features more effectively. OOD-GCL (Li et al., 2024a) also utilizes contrastive learning to learn invariant features, however, it aims to learn invariant features without labeled data, which is inherently more challenging. As illustrated in Table 1, LIRS outperforms OOD-GCL across all the datasets, likely due to that LIRS has access to labeled data during training, while OOD-GCL uses labeled data only to fine-tune the linear layer. We also compare LIRS with RSC Huang et al. (2020) and DiverseModel Teney et al. (2022), which aim to learn diverse features via ERM. LIRS can be viewed as a diverse feature learning method, as it seeks to learn more invariant features by removing spurious ones. The key distinction between LIRS and these two methods lies in that: while RSC and DiverseModel propose different regularization terms to ERM to capture diverse features, LIRS focuses on removing spurious features from ERM-learned features. As illustrated in Table 1, although RSC and DiverseModel perform well on real-world datasets, they achieve suboptimal results on the GOOD-Motif datasets. This discrepancy may arise from the fact that these methods attempt to capture diverse features, while in the GOOD-Motif datasets, only one invariant subgraph is causally related to the target. As a result, these methods may mistakenly capture non-generalizable patterns in G_s. In contrast, LIRS leverages biased infomax to effectively learn spurious patterns and subsequently identify the invariant subgraph by unlearning the spurious patterns. Lastly, LIRS significantly outperforms other OOD methods that aim to directly learn invariant features, showcasing the efficacy of the proposed learning paradigm.

Real-world datasets. In real-world datasets, which present more complex and realistic distribution shifts, many graph OOD algorithms exhibit instability, occasionally underperforming ERM. In contrast, LIRS adopts an indirect learning paradigm, which may enable the learning of more invariant features compared to previous graph invariant learning methods, leading to more effective OOD generalization. Similarly to the results on synthetic datasets, LIRS also demonstrates superior OOD performance under both scaffold shift and size shift compared to other methods. EQuAD, which adopts a similar learning paradigm as LIRS, shows a comparable trend, with a more significant advantage under the size shift relative to other methods. Furthermore, the improvements of LIRS over EQuAD across various datasets highlights the effectiveness of the biased infomax principle and the intra-class cross-entropy loss for learning spurious features and invariant features respectively. Compared to other baselines that learns invariant features directly, LIRS outperforms the best method (AIA) by 4.62% in size shift and 1.95% in scaffold shift respectively.

5.3 In-depth Analysis

Can LIRS learn more invariant features? To further validate the quality of invariant features learned by LIRS, we curated a dataset derived from the SPMotif dataset. Specifically, we constructed a binary classification dataset where the motifs *House* and *Crane* corresponds to label 0, and *Diamond* and *Cycle* corresponds to label 1. During the construction of each class's samples, we attached both invariant subgraphs to the base subgraph with 50% chance, while in the remaining 50%, we randomly attached one invariant subgraph to the base spurious subgraph. For the test set, we randomly attached a single invariant subgraph to the base subgraph. Similar to the SPMotif dataset, the base spurious subgraph was correlated with the target labels, maintaining an equal correlation strength with the labels in the test set. In addition to evaluating LIRS against traditional methods such as IRM, VRex and their variants, we also incorporated strong graph-specific OOD baselines, including CIGA, AIA, and EQuAD for comparisons. The ex-

Table 2: Performance on the SPMotif-binary datasets under varying spurious correlations.

Method	SPMotif-binary		
	$b = 0.40$	$b = 0.60$	$b = 0.90$
ERM	74.93±3.94	72.78±3.15	63.78±4.18
IRM	76.01±4.12	70.85±4.73	66.55±4.80
VREx	79.03±1.02	73.78±1.75	65.27±6.78
GIL	77.15±3.18	73.85±2.76	68.90±7.28
GREA	79.65±6.36	73.01±7.99	69.85±0.35
CIGA	76.93±3.94	71.70±1.55	66.80±5.35
AIA	78.46±3.19	71.83±0.69	64.37±4.14
EQuAD	80.82±0.65	74.20±4.10	69.79±7.81
LIRS	**82.17±0.91**	**75.32±1.65**	**71.29±2.12**

perimental results in Table 2 demonstrate that LIRS consistently outperforms other baselines across varying spurious correlation strengths, indicating its superior ability to learn more invariant features. Similarly, EQuAD, adopting a similar learning paradigm, also achieves competitive performance in SPMotif-binary datasets. This demonstrates that learning invariant features indirectly can lead to learning a more comprehensive set of invariant features and achieving better OOD generalization ability.

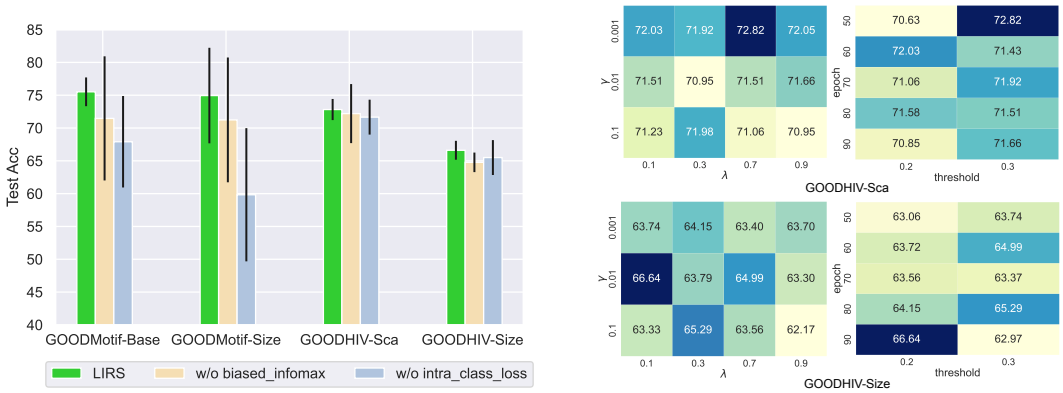

(a) Ablation study on biased infomax and intra-class cross-entropy loss.

(b) Hyperparameter sensitivity analysis on GOODHIV datasets.

Figure 4: Ablation and hyperparameter sensitivity studies for LIRS.

Ablation study. We conducted an ablation study on biased infomax and class-conditioned (intra-class) cross-entropy loss to evaluate their effectiveness in LIRS. As illustrated in Figure 4a, replacing biased infomax with vanilla infomax to generate spurious features leads to performance degradation across all datasets. This decline is primarily due to the enhanced capability of biased infomax in learning spurious features, which is crucial for subsequent steps for learning graph invariance. Furthermore, replacing class-conditioned cross-entropy loss with standard cross-entropy loss also led to negative effects, which is mainly due to the interference of spurious patterns across different classes, as discussed in Sec. 4. One typical empirical support arises from the Motif-size dataset, where each spurious pattern is correlated with different target labels with nearly equal strength. As a result, even though biased infomax can generate accurate spurious features, the logits generated using the standard cross-entropy loss are not sufficiently precise, which aligns with Prop. 2. This limitation significantly constrains the test performance, as illustrated in Figure 4a. In contrast, the class-conditioned cross-entropy loss is able to generate more accurate spurious logits, thus enhancing the OOD performance.

Hyperparameter Sensitivity. We investigate the impact of hyperparameters in LIRS, including the reweighting coefficient γ, the penalty weights λ, and hyperparameters related to biased infomax. Specifically, we analyze the effect of the epoch E at which embeddings are derived from biased infomax and the threshold used to determine whether a sample should be considered biased or not. As illustrated in Figure 4b, for both the GOODHIV-Sca and GOODHIV-Size datasets, LIRS demonstrates stable performance, highlighting its robustness to variations in hyperparameter settings. This consistency suggests that LIRS is agnostic to hyperparameter tuning, which further emphasizes its applicability in real-world scenarios.

Table 3: Performance on OGBG datasets using a different size split procedure, where the graphs in the training set have a smaller number of nodes compared to those in the test set.

Method	OGBG Datasets	
	OGBG-Molbace	OGBG-Molbbbp
ERM	76.31$\pm$0.58	87.31$\pm$2.37
IRM	79.44$\pm$3.05	88.77$\pm$2.45
VREx	76.38$\pm$1.75	84.20$\pm$2.80
GREA	77.46$\pm$5.57	86.18$\pm$2.54
GSAT	72.29$\pm$4.45	87.46$\pm$2.67
CIGA	77.89$\pm$3.68	87.94$\pm$0.86
AIA	78.62$\pm$2.88	89.18$\pm$1.77
EQuAD	82.34$\pm$3.42	88.65$\pm$3.83
LIRS	**84.62$\pm$0.84**	**90.24$\pm$4.14**

How do different size split methods affect the OOD performance? For the real-world datasets, the size split was performed in descending order, where the graphs in the training set have a larger number of nodes compared to those in the test set. To evaluate the impact of varying graph sizes on generalization ability of various OOD methods, we also performed size splits based on ascending order for the OGBG-

Molbace and OGBG-Molbbbp datasets. The results of these experiments are presented in Table 3. As shown, LIRS continues to outperform all competitive baselines under this alternative size split. Specifically, LIRS achieves the highest ROC-AUC scores on both OGBG-Molbace and OGBG-Molbbbp datasets. This highlights the superiority of LIRS in generalizing to larger graphs when trained on smaller ones, further confirming its potential for real-world applications.

6 Related Work

Learning invariant features. OOD generalization is a critical challenge in machine learning, where models trained on a specific data distribution often fail to generalize well to unseen distributions. Recently invariance learning has been proposed to tackle this issue, which builds upon the theory of causality (Peters et al., 2016; Pearl, 2009) to learn causally-related representation that remain stable across different environments (Arjovsky et al., 2020; Parascandolo et al., 2020; Mahajan et al., 2021; Wald et al., 2021; Ahuja et al., 2020; 2021). Inspired from IRM (Arjovsky et al., 2020), several invariant learning methods on graphs are proposed (Yang et al., 2022; Li et al., 2022b; Fan et al., 2022; Liu et al., 2022; Wu et al., 2022c; Chen et al., 2022; 2023a; Gui et al., 2023; Sui et al., 2023; Li et al., 2024b) to learn graph-level representations that are robust to distribution shifts. Most of these methods aim to learn invariant features directly by training an equipredictive classifier. Recent study (Yao et al., 2024) has proposed a new learning paradigm to learn graph invariance indirectly by learning spurious features first, then disentangle them from the ERM-learned representations. In this work, we adopt this learning paradigm for learning graph invariance.

Self-supervised learning induces spuriosity. Self-supervised learning (SSL) has emerged as a potent paradigm for learning representations from unlabeled datasets. The fundamental concept involves devising pretext tasks that maximize similarity between two augmented views of the same data point, often utilizing the InfoNCE loss (Oord et al., 2018). This approach has been widely applied in domains such as images (Chen et al., 2020a;b) and graphs (Veličković et al., 2019; Sun et al., 2019; Zhu et al., 2020; You et al., 2020). Recent work have shown that SSL may tend to learn spurious features in both image domain (Hamidieh et al., 2024; Meehan et al., 2023) and graph domain (Yao et al., 2024). Hamidieh et al. (2024) attempted to enhance SSL model performance by addressing this issue and promoting the learning of invariant features. In contrast, our goal in this work is to improve SSL model ability to capture spuriosity, thereby facilitating better feature disentanglement for invariant learning.

Learning diverse features. Recent studies have shown that ERM tends to encourage models to learn the simplest predictive features (Hermann & Lampinen, 2020; Kalimeris et al., 2019; Neyshabur et al., 2014; Pezeshki et al., 2021). This simplicity bias causes the models to rely on simple (spurious) but non-causal features, ignoring more complex patterns that might be equally predictive. To address this challenge, Huang et al. (2020) employs a self-challenging mechanism to force the model to learn diverse patterns by discarding dominant features, while Teney et al. (2022) constructs diverse features by training a collection of classifiers with diversity regularization. Additionally, Zhang et al. (2022a); Chen et al. (2023b) adopt DRO to iteratively explore new features. While previous works aim to encourage models to learn a diverse set of predictive patterns, our method takes a different approach. Specifically, we aim to remove or unlearn spurious features from ERM-learned features, thereby allowing the model to capture more invariant features.

7 Conclusions

In this study, we identified a critical limitation in IRM, VRex and their variants on graph invariant learning, i.e., these methods may only capture a subset of the invariant features, thereby limiting their OOD generalization performance. To address this issue, we investigate the effectiveness of learning invariant features *indirectly* by first learning and then removing spurious features. Our theoretical and empirical analyses demonstrate that this approach facilitates the learning of a more comprehensive set of invariant features than traditional (graph) invariant learning methods, thereby improving generalization to unseen environments. We then propose **LIRS** that adopts this learning paradigm, which consists of: a) The biased infomax principle, and b) The class-conditioned cross-entropy loss, which elicit effective spuriosity learning and invariant learning respectively, aiming to learn more invariant features. Extensive experiments on both synthetic and real-world datasets demonstrate the superiority of our proposed method over existing state-of-the-art OOD algorithms.

REFERENCES

Kartik Ahuja, Karthikeyan Shanmugam, Kush Varshney, and Amit Dhurandhar. Invariant risk minimization games. In *International Conference on Machine Learning*, pp. 145–155. PMLR, 2020.

Kartik Ahuja, Ethan Caballero, Dinghuai Zhang, Jean-Christophe Gagnon-Audet, Yoshua Bengio, Ioannis Mitliagkas, and Irina Rish. Invariance principle meets information bottleneck for out-of-distribution generalization. *Advances in Neural Information Processing Systems*, 34:3438–3450, 2021.

Martin Arjovsky, Léon Bottou, Ishaan Gulrajani, and David Lopez-Paz. Invariant risk minimization, 2020.

Steve Azzolin, Antonio Longa, Pietro Barbiero, Pietro Liò, and Andrea Passerini. Global explainability of gnns via logic combination of learned concepts. *arXiv preprint arXiv:2210.07147*, 2022.

Guy W Bemis and Mark A Murcko. The properties of known drugs. 1. molecular frameworks. *Journal of medicinal chemistry*, 39(15):2887–2893, 1996.

Ngoc Bui, Hieu Trung Nguyen, Viet Anh Nguyen, and Rex Ying. Explaining graph neural networks via structure-aware interaction index. *arXiv preprint arXiv:2405.14352*, 2024.

Ting Chen, Simon Kornblith, Mohammad Norouzi, and Geoffrey Hinton. A simple framework for contrastive learning of visual representations. In *International conference on machine learning*, pp. 1597–1607. PMLR, 2020a.

Xinlei Chen, Haoqi Fan, Ross Girshick, and Kaiming He. Improved baselines with momentum contrastive learning. *arXiv preprint arXiv:2003.04297*, 2020b.

Yongqiang Chen, Yonggang Zhang, Yatao Bian, Han Yang, MA Kaili, Binghui Xie, Tongliang Liu, Bo Han, and James Cheng. Learning causally invariant representations for out-of-distribution generalization on graphs. *Advances in Neural Information Processing Systems*, 35:22131–22148, 2022.

Yongqiang Chen, Yatao Bian, Kaiwen Zhou, Binghui Xie, Bo Han, and James Cheng. Does invariant graph learning via environment augmentation learn invariance? In *Thirty-seventh Conference on Neural Information Processing Systems*, 2023a. URL `https://openreview.net/forum?id=EqpR9Vtt13`.

Yongqiang Chen, Wei Huang, Kaiwen Zhou, Yatao Bian, Bo Han, and James Cheng. Understanding and improving feature learning for out-of-distribution generalization. *Advances in Neural Information Processing Systems*, 36, 2023b.

Alex J. DeGrave, Joseph D. Janizek, and Su-In Lee. Ai for radiographic covid-19 detection selects shortcuts over signal. *medRxiv*, 2020. URL `https://api.semanticscholar.org/CorpusID:221653623`.

Qi Dou, Daniel Coelho de Castro, Konstantinos Kamnitsas, and Ben Glocker. Domain generalization via model-agnostic learning of semantic features. *Advances in neural information processing systems*, 32, 2019.

Cian Eastwood, Shashank Singh, Andrei L Nicolicioiu, Marin Vlastelica Pogančić, Julius von Kügelgen, and Bernhard Schölkopf. Spuriosity didn't kill the classifier: Using invariant predictions to harness spurious features. *Advances in Neural Information Processing Systems*, 36, 2023.

Shaohua Fan, Xiao Wang, Yanhu Mo, Chuan Shi, and Jian Tang. Debiasing graph neural networks via learning disentangled causal substructure. *Advances in Neural Information Processing Systems*, 35:24934–24946, 2022.

Matthias Fey and Jan Eric Lenssen. Fast graph representation learning with pytorch geometric, 2019.

Yaroslav Ganin, Evgeniya Ustinova, Hana Ajakan, Pascal Germain, Hugo Larochelle, François Laviolette, Mario March, and Victor Lempitsky. Domain-adversarial training of neural networks. *Journal of machine learning research*, 17(59):1–35, 2016.

Shurui Gui, Xiner Li, Limei Wang, and Shuiwang Ji. GOOD: A graph out-of-distribution benchmark. In *Thirty-sixth Conference on Neural Information Processing Systems Datasets and Benchmarks Track*, 2022. URL https://openreview.net/forum?id=8hHg-zs_p-h.

Shurui Gui, Meng Liu, Xiner Li, Youzhi Luo, and Shuiwang Ji. Joint learning of label and environment causal independence for graph out-of-distribution generalization. *Advances in Neural Information Processing Systems*, 36, 2023.

Kimia Hamidieh, Haoran Zhang, Swami Sankaranarayanan, and Marzyeh Ghassemi. Views can be deceiving: Improved SSL through feature space augmentation. In *The Twelfth International Conference on Learning Representations*, 2024. URL https://openreview.net/forum?id=mutJBk3ILg.

Kaveh Hassani and Amir Hosein Khasahmadi. Contrastive multi-view representation learning on graphs. In *International conference on machine learning*, pp. 4116–4126. PMLR, 2020.

Katherine Hermann and Andrew Lampinen. What shapes feature representations? exploring datasets, architectures, and training. *Advances in Neural Information Processing Systems*, 33: 9995–10006, 2020.

R Devon Hjelm, Alex Fedorov, Samuel Lavoie-Marchildon, Karan Grewal, Phil Bachman, Adam Trischler, and Yoshua Bengio. Learning deep representations by mutual information estimation and maximization, 2019.

Weihua Hu, Gang Niu, Issei Sato, and Masashi Sugiyama. Does distributionally robust supervised learning give robust classifiers? In *International Conference on Machine Learning*, pp. 2029–2037. PMLR, 2018.

Weihua Hu, Matthias Fey, Marinka Zitnik, Yuxiao Dong, Hongyu Ren, Bowen Liu, Michele Catasta, and Jure Leskovec. Open graph benchmark: Datasets for machine learning on graphs. *Advances in neural information processing systems*, 33:22118–22133, 2020.

Kexin Huang, Tianfan Fu, Wenhao Gao, Yue Zhao, Yusuf Roohani, Jure Leskovec, Connor W Coley, Cao Xiao, Jimeng Sun, and Marinka Zitnik. Therapeutics data commons: Machine learning datasets and tasks for drug discovery and development. *arXiv preprint arXiv:2102.09548*, 2021.

Zeyi Huang, Haohan Wang, Eric P Xing, and Dong Huang. Self-challenging improves cross-domain generalization. In *Computer vision–ECCV 2020: 16th European conference, Glasgow, UK, August 23–28, 2020, proceedings, part II 16*, pp. 124–140. Springer, 2020.

Yuanfeng Ji, Lu Zhang, Jiaxiang Wu, Bingzhe Wu, Long-Kai Huang, Tingyang Xu, Yu Rong, Lanqing Li, Jie Ren, Ding Xue, et al. Drugood: Out-of-distribution (ood) dataset curator and benchmark for ai-aided drug discovery–a focus on affinity prediction problems with noise annotations. *arXiv preprint arXiv:2201.09637*, 2022.

Dimitris Kalimeris, Gal Kaplun, Preetum Nakkiran, Benjamin Edelman, Tristan Yang, Boaz Barak, and Haofeng Zhang. Sgd on neural networks learns functions of increasing complexity. *Advances in neural information processing systems*, 32, 2019.

Prannay Khosla, Piotr Teterwak, Chen Wang, Aaron Sarna, Yonglong Tian, Phillip Isola, Aaron Maschinot, Ce Liu, and Dilip Krishnan. Supervised contrastive learning. *Advances in neural information processing systems*, 33:18661–18673, 2020.

Diederik P Kingma and Jimmy Ba. Adam: A method for stochastic optimization. *arXiv preprint arXiv:1412.6980*, 2014.

Thomas N. Kipf and Max Welling. Semi-supervised classification with graph convolutional networks. In *International Conference on Learning Representations*, 2017. URL https://openreview.net/forum?id=SJU4ayYgl.

Polina Kirichenko, Pavel Izmailov, and Andrew Gordon Wilson. Last layer re-training is sufficient for robustness to spurious correlations, 2023.

Pang Wei Koh, Shiori Sagawa, Henrik Marklund, Sang Michael Xie, Marvin Zhang, Akshay Balsubramani, Weihua Hu, Michihiro Yasunaga, Richard Lanas Phillips, Irena Gao, et al. Wilds: A benchmark of in-the-wild distribution shifts. In *International conference on machine learning*, pp. 5637–5664. PMLR, 2021.

Kezhi Kong, Guohao Li, Mucong Ding, Zuxuan Wu, Chen Zhu, Bernard Ghanem, Gavin Taylor, and Tom Goldstein. Robust optimization as data augmentation for large-scale graphs. In *Proceedings of the IEEE/CVF conference on computer vision and pattern recognition*, pp. 60–69, 2022.

Devin Kreuzer, Dominique Beaini, Will Hamilton, Vincent Létourneau, and Prudencio Tossou. Rethinking graph transformers with spectral attention. *Advances in Neural Information Processing Systems*, 34:21618–21629, 2021.

David Krueger, Ethan Caballero, Joern-Henrik Jacobsen, Amy Zhang, Jonathan Binas, Dinghuai Zhang, Remi Le Priol, and Aaron Courville. Out-of-distribution generalization via risk extrapolation (rex). In *International Conference on Machine Learning*, pp. 5815–5826. PMLR, 2021.

Haoyang Li, Xin Wang, Ziwei Zhang, and Wenwu Zhu. Ood-gnn: Out-of-distribution generalized graph neural network. *IEEE Transactions on Knowledge and Data Engineering*, 2022a.

Haoyang Li, Ziwei Zhang, Xin Wang, and Wenwu Zhu. Learning invariant graph representations for out-of-distribution generalization. In Alice H. Oh, Alekh Agarwal, Danielle Belgrave, and Kyunghyun Cho (eds.), *Advances in Neural Information Processing Systems*, 2022b. URL https://openreview.net/forum?id=acKK8MQe2xc.

Haoyang Li, Ziwei Zhang, Xin Wang, and Wenwu Zhu. Invariant node representation learning under distribution shifts with multiple latent environments. *ACM Transactions on Information Systems*, 42(1):1–30, 2023a.

Haoyang Li, Xin Wang, Zeyang Zhang, Haibo Chen, Ziwei Zhang, and Wenwu Zhu. Disentangled graph self-supervised learning for out-of-distribution generalization. In *Forty-first International Conference on Machine Learning*, 2024a.

Xiner Li, Shurui Gui, Youzhi Luo, and Shuiwang Ji. Graph structure and feature extrapolation for out-of-distribution generalization. *arXiv preprint arXiv:2306.08076*, 2023b.

Xiner Li, Shurui Gui, Youzhi Luo, and Shuiwang Ji. Graph structure extrapolation for out-of-distribution generalization. In *Forty-first International Conference on Machine Learning*, 2024b. URL https://openreview.net/forum?id=Xgrey8uQhr.

Ya Li, Xinmei Tian, Mingming Gong, Yajing Liu, Tongliang Liu, Kun Zhang, and Dacheng Tao. Deep domain generalization via conditional invariant adversarial networks. In *Proceedings of the European conference on computer vision (ECCV)*, pp. 624–639, 2018.

R. Linsker. Self-organization in a perceptual network. *Computer*, 21(3):105–117, 1988. doi: 10.1109/2.36.

Gang Liu, Tong Zhao, Jiaxin Xu, Tengfei Luo, and Meng Jiang. Graph rationalization with environment-based augmentations. In *Proceedings of the 28th ACM SIGKDD Conference on Knowledge Discovery and Data Mining*, KDD '22. ACM, August 2022. doi: 10.1145/3534678.3539347. URL http://dx.doi.org/10.1145/3534678.3539347.

Yang Liu, Xiang Ao, Fuli Feng, Yunshan Ma, Kuan Li, Tat-Seng Chua, and Qing He. Flood: A flexible invariant learning framework for out-of-distribution generalization on graphs. In *Proceedings of the 29th ACM SIGKDD Conference on Knowledge Discovery and Data Mining*, pp. 1548–1558, 2023.

Dongsheng Luo, Wei Cheng, Dongkuan Xu, Wenchao Yu, Bo Zong, Haifeng Chen, and Xiang Zhang. Parameterized explainer for graph neural network. *Advances in neural information processing systems*, 33:19620–19631, 2020.

Divyat Mahajan, Shruti Tople, and Amit Sharma. Domain generalization using causal matching. In *International conference on machine learning*, pp. 7313–7324. PMLR, 2021.

Casey Meehan, Florian Bordes, Pascal Vincent, Kamalika Chaudhuri, and Chuan Guo. Do ssl models have déjà vu? a case of unintended memorization in self-supervised learning. *Advances in Neural Information Processing Systems*, 36, 2023.

Siqi Miao, Mia Liu, and Pan Li. Interpretable and generalizable graph learning via stochastic attention mechanism. In *International Conference on Machine Learning*, pp. 15524–15543. PMLR, 2022.

Hongseok Namkoong and John C. Duchi. Stochastic gradient methods for distributionally robust optimization with f-divergences. In *Proceedings of the 30th International Conference on Neural Information Processing Systems*, NIPS'16, pp. 2216–2224, Red Hook, NY, USA, 2016. Curran Associates Inc. ISBN 9781510838819.

Behnam Neyshabur, Ryota Tomioka, and Nathan Srebro. In search of the real inductive bias: On the role of implicit regularization in deep learning. *arXiv preprint arXiv:1412.6614*, 2014.

Aaron van den Oord, Yazhe Li, and Oriol Vinyals. Representation learning with contrastive predictive coding. *arXiv preprint arXiv:1807.03748*, 2018.

Giambattista Parascandolo, Alexander Neitz, Antonio Orvieto, Luigi Gresele, and Bernhard Schölkopf. Learning explanations that are hard to vary. *arXiv preprint arXiv:2009.00329*, 2020.

Adam Paszke, Sam Gross, Francisco Massa, Adam Lerer, James Bradbury, Gregory Chanan, Trevor Killeen, Zeming Lin, Natalia Gimelshein, Luca Antiga, Alban Desmaison, Andreas Köpf, Edward Yang, Zach DeVito, Martin Raison, Alykhan Tejani, Sasank Chilamkurthy, Benoit Steiner, Lu Fang, Junjie Bai, and Soumith Chintala. Pytorch: An imperative style, high-performance deep learning library, 2019.

Judea Pearl. *Causality*. Cambridge University Press, Cambridge, UK, 2 edition, 2009. ISBN 978-0-521-89560-6. doi: 10.1017/CBO9780511803161.

F. Pedregosa, G. Varoquaux, A. Gramfort, V. Michel, B. Thirion, O. Grisel, M. Blondel, P. Prettenhofer, R. Weiss, V. Dubourg, J. Vanderplas, A. Passos, D. Cournapeau, M. Brucher, M. Perrot, and E. Duchesnay. Scikit-learn: Machine learning in Python. *Journal of Machine Learning Research*, 12:2825–2830, 2011.

Jonas Peters, Peter Bühlmann, and Nicolai Meinshausen. Causal inference by using invariant prediction: identification and confidence intervals. *Journal of the Royal Statistical Society Series B: Statistical Methodology*, 78(5):947–1012, 2016.

Mohammad Pezeshki, Oumar Kaba, Yoshua Bengio, Aaron C Courville, Doina Precup, and Guillaume Lajoie. Gradient starvation: A learning proclivity in neural networks. *Advances in Neural Information Processing Systems*, 34:1256–1272, 2021.

Phillip E Pope, Soheil Kolouri, Mohammad Rostami, Charles E Martin, and Heiko Hoffmann. Explainability methods for graph convolutional neural networks. In *Proceedings of the IEEE/CVF conference on computer vision and pattern recognition*, pp. 10772–10781, 2019.

Jiezhong Qiu, Jian Tang, Hao Ma, Yuxiao Dong, Kuansan Wang, and Jie Tang. Deepinf: Social influence prediction with deep learning. In *Proceedings of the 24th ACM SIGKDD International Conference on Knowledge Discovery amp; Data Mining*, KDD '18. ACM, July 2018. doi: 10.1145/3219819.3220077. URL `http://dx.doi.org/10.1145/3219819.3220077`.

Yu Rong, Wenbing Huang, Tingyang Xu, and Junzhou Huang. Dropedge: Towards deep graph convolutional networks on node classification. *arXiv preprint arXiv:1907.10903*, 2019.

Shiori Sagawa, Pang Wei Koh, Tatsunori B Hashimoto, and Percy Liang. Distributionally robust neural networks for group shifts: On the importance of regularization for worst-case generalization. *arXiv preprint arXiv:1911.08731*, 2019.

Thomas Schnake, Oliver Eberle, Jonas Lederer, Shinichi Nakajima, Kristof T Schütt, Klaus-Robert Müller, and Grégoire Montavon. Higher-order explanations of graph neural networks via relevant walks. *IEEE transactions on pattern analysis and machine intelligence*, 44(11):7581–7596, 2021.

Yongduo Sui, Qitian Wu, Jiancan Wu, Qing Cui, Longfei Li, Jun Zhou, Xiang Wang, and Xiangnan He. Unleashing the power of graph data augmentation on covariate distribution shift. *Advances in Neural Information Processing Systems*, 36, 2023.

Baochen Sun and Kate Saenko. Deep coral: Correlation alignment for deep domain adaptation, 2016.

Fan-Yun Sun, Jordan Hoffmann, Vikas Verma, and Jian Tang. Infograph: Unsupervised and semi-supervised graph-level representation learning via mutual information maximization. *arXiv preprint arXiv:1908.01000*, 2019.

Damien Teney, Ehsan Abbasnejad, Simon Lucey, and Anton Van den Hengel. Evading the simplicity bias: Training a diverse set of models discovers solutions with superior ood generalization. In *Proceedings of the IEEE/CVF conference on computer vision and pattern recognition*, pp. 16761–16772, 2022.

George R Terrell and David W Scott. Variable kernel density estimation. *The Annals of Statistics*, pp. 1236–1265, 1992.

Naftali Tishby and Noga Zaslavsky. Deep learning and the information bottleneck principle, 2015.

Laurens Van der Maaten and Geoffrey Hinton. Visualizing data using t-sne. *Journal of machine learning research*, 9(11), 2008.

Vladimir N. Vapnik. *The nature of statistical learning theory*. Springer-Verlag New York, Inc., 1995. ISBN 0-387-94559-8.

Petar Veličković, Guillem Cucurull, Arantxa Casanova, Adriana Romero, Pietro Lio, and Yoshua Bengio. Graph attention networks. *arXiv preprint arXiv:1710.10903*, 2017.

Petar Veličković, William Fedus, William L Hamilton, Pietro Liò, Yoshua Bengio, and R Devon Hjelm. Deep graph infomax. *arXiv preprint arXiv:1809.10341*, 2018.

Petar Veličković, William Fedus, William L. Hamilton, Pietro Liò, Yoshua Bengio, and R Devon Hjelm. Deep graph infomax. In *International Conference on Learning Representations*, 2019. URL `https://openreview.net/forum?id=rklz9iAcKQ`.

Yoav Wald, Amir Feder, Daniel Greenfeld, and Uri Shalit. On calibration and out-of-domain generalization. In A. Beygelzimer, Y. Dauphin, P. Liang, and J. Wortman Vaughan (eds.), *Advances in Neural Information Processing Systems*, 2021. URL `https://openreview.net/forum?id=XWYJ25-yTRS`.

Xiaoqi Wang and Han-Wei Shen. Gnninterpreter: A probabilistic generative model-level explanation for graph neural networks. *arXiv preprint arXiv:2209.07924*, 2022.

Qitian Wu, Hengrui Zhang, Junchi Yan, and David Wipf. Handling distribution shifts on graphs: An invariance perspective, 2022a.

Shiwen Wu, Fei Sun, Wentao Zhang, Xu Xie, and Bin Cui. Graph neural networks in recommender systems: A survey. *ACM Comput. Surv.*, 55(5), dec 2022b. ISSN 0360-0300. doi: 10.1145/3535101. URL `https://doi.org/10.1145/3535101`.

Yingxin Wu, Xiang Wang, An Zhang, Xiangnan He, and Tat-Seng Chua. Discovering invariant rationales for graph neural networks. In *International Conference on Learning Representations*, 2022c. URL `https://openreview.net/forum?id=hGXij5rfiHw`.

Zhenqin Wu, Bharath Ramsundar, Evan N. Feinberg, Joseph Gomes, Caleb Geniesse, Aneesh S. Pappu, Karl Leswing, and Vijay Pande. Moleculenet: A benchmark for molecular machine learning, 2018.

Keyulu Xu, Weihua Hu, Jure Leskovec, and Stefanie Jegelka. How powerful are graph neural networks? *arXiv preprint arXiv:1810.00826*, 2018.

Keyulu Xu, Weihua Hu, Jure Leskovec, and Stefanie Jegelka. How powerful are graph neural networks? In *International Conference on Learning Representations*, 2019. URL https://openreview.net/forum?id=ryGs6iA5Km.

Nianzu Yang, Kaipeng Zeng, Qitian Wu, Xiaosong Jia, and Junchi Yan. Learning substructure invariance for out-of-distribution molecular representations. In Alice H. Oh, Alekh Agarwal, Danielle Belgrave, and Kyunghyun Cho (eds.), *Advances in Neural Information Processing Systems*, 2022. URL https://openreview.net/forum?id=2nWUNTnFijm.

Huaxiu Yao, Yu Wang, Sai Li, Linjun Zhang, Weixin Liang, James Zou, and Chelsea Finn. Improving out-of-distribution robustness via selective augmentation. In *International Conference on Machine Learning*, pp. 25407–25437. PMLR, 2022.

Tianjun Yao, Yongqiang Chen, Zhenhao Chen, Kai Hu, Zhiqiang Shen, and Kun Zhang. Empowering graph invariance learning with deep spurious infomax. In *Forty-first International Conference on Machine Learning*, 2024. URL https://openreview.net/forum?id=u9oSQtujCF.

Zhitao Ying, Dylan Bourgeois, Jiaxuan You, Marinka Zitnik, and Jure Leskovec. Gnnexplainer: Generating explanations for graph neural networks. *Advances in neural information processing systems*, 32, 2019.

Yuning You, Tianlong Chen, Yongduo Sui, Ting Chen, Zhangyang Wang, and Yang Shen. Graph contrastive learning with augmentations. *Advances in neural information processing systems*, 33: 5812–5823, 2020.

Bing Yu, Haoteng Yin, and Zhanxing Zhu. Spatio-temporal graph convolutional networks: A deep learning framework for traffic forecasting. In *Proceedings of the Twenty-Seventh International Joint Conference on Artificial Intelligence*, IJCAI-2018. International Joint Conferences on Artificial Intelligence Organization, July 2018. doi: 10.24963/ijcai.2018/505. URL http://dx.doi.org/10.24963/ijcai.2018/505.

Junchi Yu, Jian Liang, and Ran He. Mind the label shift of augmentation-based graph ood generalization. In *Proceedings of the IEEE/CVF Conference on Computer Vision and Pattern Recognition*, pp. 11620–11630, 2023.

Hao Yuan, Jiliang Tang, Xia Hu, and Shuiwang Ji. Xgnn: Towards model-level explanations of graph neural networks. In *Proceedings of the 26th ACM SIGKDD international conference on knowledge discovery & data mining*, pp. 430–438, 2020.

Jianyu Zhang, David Lopez-Paz, and Léon Bottou. Rich feature construction for the optimization-generalization dilemma. In *International Conference on Machine Learning*, pp. 26397–26411. PMLR, 2022a.

Michael Zhang, Nimit S Sohoni, Hongyang R Zhang, Chelsea Finn, and Christopher Ré. Correct-n-contrast: A contrastive approach for improving robustness to spurious correlations. *arXiv preprint arXiv:2203.01517*, 2022b.

Zehong Zhang, Lifan Chen, Feisheng Zhong, Dingyan Wang, Jiaxin Jiang, Sulin Zhang, Hualiang Jiang, Mingyue Zheng, and Xutong Li. Graph neural network approaches for drug-target interactions. *Current Opinion in Structural Biology*, 73:102327, 2022c. ISSN 0959-440X. doi: https://doi.org/10.1016/j.sbi.2021.102327. URL https://www.sciencedirect.com/science/article/pii/S0959440X2100169X.

Zhilu Zhang and Mert R. Sabuncu. Generalized cross entropy loss for training deep neural networks with noisy labels, 2018.

Yanqiao Zhu, Yichen Xu, Feng Yu, Qiang Liu, Shu Wu, and Liang Wang. Deep graph contrastive representation learning. *arXiv preprint arXiv:2006.04131*, 2020.

Yanqiao Zhu, Yichen Xu, Qiang Liu, and Shu Wu. An Empirical Study of Graph Contrastive Learning. *arXiv.org*, September 2021.

Xiang Zhuang, Qiang Zhang, Keyan Ding, Yatao Bian, Xiao Wang, Jingsong Lv, Hongyang Chen, and Huajun Chen. Learning invariant molecular representation in latent discrete space. *Advances in Neural Information Processing Systems*, 36, 2023.

APPENDIX

A NOTATIONS

We present a set of notations used throughout our paper for clarity. Below are the main notations along with their definitions.

Table 4: Notation Table

Symbols	Definitions
$\mathcal{G}$	a set of graphs
$G = (A, X)$	a graph with the adjacency matrix $A \in \{0,1\}^{n\times n}$ and node feature matrix $X \in \mathbb{R}^{n\times d}$
Y	random variable for labels
C	content factor
S	style factor
E	environment
$\mathbf{h}_c$	invariant representations (features)
$\mathbf{h}_s$	spurious representations (features)
G_c	the invariant subgraph with respect to G
G_s	the spurious subgraph with respect to G
$\widehat{G}_c$	the estimated invariant subgraph
$\widehat{G}_s$	the estimated spurious subgraph
$\widehat{\mathbf{h}}_G$	the estimated graph representation for graph G
$\widehat{\mathbf{h}}_i$	the estimated node representation for node $i \in G$
$\widehat{\mathbf{h}}_c$	the estimated invariant graph representation, interchangeably with $\widehat{C}$ in our paper
$\widehat{\mathbf{h}}_s$	the estimated spurious graph representation, interchangeably with $\widehat{S}$ in our paper
$\mathbf{s}_j^{(i)}$	The jth entry of the spurious logits derived from $\mathbf{h}_s^{(i)}$ for sample $G^{(i)}$
$\widehat{\mathbf{s}}_j^{(i)}$	The jth of the estimated spurious logits for sample $G^{(i)}$
$h(\cdot)$	encoder
$\rho(\cdot)$	classification head for $\mathcal{L}_{GT}$
$\rho'(\cdot)$	classification head for $\mathcal{L}_{Inv}$
$w^{(i)}$	reweighting coefficient for sample $G^{(i)}$
$[K] := \{1, 2, \cdots, K\}$	index set with K elements
$\mathbf{1}_K$	all-one (column) vector with K entries
$\mathbf{w}$	a vector
$\mathbf{W}$	a matrix
W	a random variable
$\mathcal{W}$	a set

B MORE BACKGROUND AND PRELIMINARIES

Graph Neural Networks. In this work, we adopt message-passing GNNs for graph classification due to their expressiveness. Given a simple and undirected graph $G = (\mathbf{A}, \mathbf{X})$ with n nodes and m edges, where $\mathbf{A} \in \{0,1\}^{n\times n}$ is the adjacency matrix, and $\mathbf{X} \in \mathbb{R}^{n\times d}$ is the node feature matrix with d feature dimensions, the graph encoder $h : \mathbb{G} \to \mathbb{R}^h$ aims to learn a meaningful graph-level representation h_G, and the classifier $\rho : \mathbb{R}^h \to \mathbb{Y}$ is used to predict the graph label $\widehat{Y}_G = \rho(h_G)$. To obtain the graph representation h_G, the representation $\mathbf{h}_v^{(l)}$ of each node v in a graph G is iteratively updated by aggregating information from its neighbors $\mathcal{N}(v)$. For the l-th layer, the updated representation is obtained via an AGGREGATE operation followed by an UPDATE operation:

$$\mathbf{m}_v^{(l)} = \text{AGGREGATE}^{(l)}\left(\left\{\mathbf{h}_u^{(l-1)} : u \in \mathcal{N}(v)\right\}\right), \tag{5}$$

$$\mathbf{h}_v^{(l)} = \text{UPDATE}^{(l)}\left(\mathbf{h}_v^{(l-1)}, \mathbf{m}_v^{(l)}\right), \tag{6}$$

where $\mathbf{h}_v^{(0)} = \mathbf{x}_v$ is the initial node feature of node v in graph G. Then GNNs employ a READOUT function to aggregate the final layer node features $\left\{\mathbf{h}_v^{(L)} : v \in \mathcal{V}\right\}$ into a graph-level representation $\mathbf{h}_G$:

$$\mathbf{h}_G = \mathrm{READOUT}\left(\left\{\mathbf{h}_v^{(L)} : v \in \mathcal{V}\right\}\right). \tag{7}$$

Data Generating Process. The presumed data generating process adopted in this work is similar to the previous studies (Arjovsky et al., 2020; Ahuja et al., 2020; Chen et al., 2022; 2023a; Wu et al., 2022a). The dynamics of graph generation are fundamentally grounded upon the principles of Structural Causal Models (SCM) (Peters et al., 2016), capturing the complex interplay between latent variables and their influence on observable graph characteristics. This model assumes the graph generation as a function $f_{\text{gen}} : \mathbb{Z} \to \mathbb{G}$, where $\mathbb{Z} \subseteq \mathbb{R}^n$ denotes the latent space, and $\mathbb{G}$ is the graph space. Through the lens of SCM, the generation process is decomposed into the invariant subgraph G_c, the spurious subgraph G_s, and the observed graph G respectively, as formulated in the following equation:

$$G_c := f_{\text{gen}}^{G_c}(C), \quad G_s := f_{\text{gen}}^{G_s}(S), \quad G := f_{\text{gen}}^{G}(G_c, G_s).$$

Furthermore, the latent interactions among C, S, and Y can exhibit two types of conditional independence: (i) $Y \perp\!\!\!\perp S \mid C$ and (ii) $Y \not\perp\!\!\!\perp S \mid C$. In case (i), the invariant factor C is fully informative (FIIF) to the target label Y, and the latent spurious factor S provide no further information. In case (ii), the invariant factor C is only partially informative (PIIF) about Y, spurious factor S can further provide additional information to aid the prediction of Y, however, as S is directly affected by E, it is not stable across different environments. The SCMs for the two scenarios are illustrated in Figure 5. For the PIIF SCM, the structure equation is:

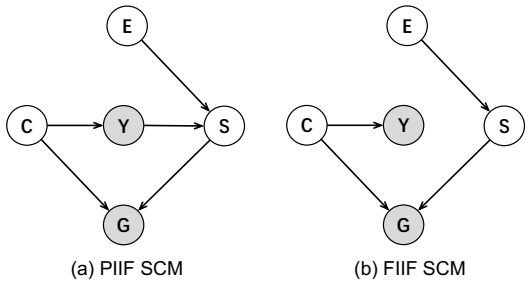

Figure 5: Structure causal models for graph data generation.

$$Y = X_c + n_1, X_s = Y + n_2 + \epsilon^e, \tag{8}$$

while for FIIF SCM, the structure equation is:

$$Y = X_c + n_1, X_s = n_2 + \epsilon^e. \tag{9}$$

Here X_c and X_s denote the random variables for invariant factor and spurious factor respectively. n_1 and n_2 represent random Gaussian noise, and ϵ^e stands for an environmental variable, which causes the spurious correlation between X_s and Y.

C Additional Related Work

OOD Generalization. OOD generalization is a critical challenge in machine learning, where models trained on a specific data distribution often fail to generalize well to unseen distributions. Several approaches have been proposed to address this issue, including domain generalization, distributional robustness optimization (DRO), and invariance learning. *Domain generalization* aims to learn features that are invariant across different domains or environments. Previous studies, such as Ganin et al. (2016); Sun & Saenko (2016); Li et al. (2018); Dou et al. (2019), regularize the learned features to be domain-invariant. *DRO* methods focus on training models to perform robust against the worst-case scenarios among diverse data groups. Namkoong & Duchi (2016); Hu et al. (2018); Sagawa et al. (2019) regularize models to be robust to mild distributional perturbations of the training distributions, expecting the models to perform well in unseen test environments. Building upon this, Liu et al. (2022) Zhang et al. (2022b) and Yao et al. (2022) propose advanced strategies to improve robustness by assuming that models trained with ERM have a strong reliance on spurious features.

Invariance learning leverages the theory of causality (Peters et al., 2016; Pearl, 2009) and introduces causal invariance to the learned representations. The Independent Causal Mechanism (ICM) assumption in causality states that the conditional distribution of each variable given its causes does not inform or influence other conditional distributions. Despite changes to the intervened variables, the conditional distribution of intervened variables and the target variable remains invariant. Arjovsky et al. (2020) proposes the framework of Invariant Risk Minimization (IRM) that allows the adoption of causal invariance in deep neural networks, inspiring various invariant learning works such as Parascandolo et al. (2020); Mahajan et al. (2021); Wald et al. (2021); Ahuja et al. (2020; 2021); Krueger et al. (2021).

Graph-Level OOD Generalization. Recently, there has been a growing interest in learning graph-level representations that are robust under distribution shifts, particularly from the perspective of invariant learning. MoleOOD Yang et al. (2022) and GIL Li et al. (2022b) propose to infer environmental labels to assist in identifying invariant substructures within graphs. DIR Wu et al. (2022c), GREA Liu et al. (2022) and iMoLD Zhuang et al. (2023) employ environment augmentation techniques to facilitate the learning of invariant graph-level representations. These methods typically rely on the explicit manipulation of unobserved environmental variables to achieve generalization across unseen distributions. AIA Sui et al. (2023) employs an adversarial augmenter to explore OOD data by generating new environments while maintaining stable feature consistency. To circumvent the need for environmental inference or augmentation, CIGA Chen et al. (2022) and GALA Chen et al. (2023a) utilizes supervised contrastive learning to identify invariant subgraphs based on the assumption that samples sharing the same label exhibit similar invariant subgraphs. EQuAD Yao et al. (2024) adopts self-supervised learning to learn spuriosu efatures first, followed by learning invariant features by unlearning spurious features. LECI Gui et al. (2023) and G-Splice Li et al. (2023b) assume the availability of environment labels, and study environment exploitation strategies for graph OOD generalization. LECI Gui et al. (2023) proposes to learn a causal subgraph selector by jointly optimizing label and environment causal independence, and G-Splice Li et al. (2023b) studies graph and feature space extrapolation for environment augmentation, which maintains causal validity. On the other hand, some works do not utilize the invariance principle for graph OOD generalization. DisC Fan et al. (2022) initially learns a biased graph representation and subsequently focuses on unbiased graphs to discover invariant subgraphs. GSAT Miao et al. (2022) utilizes information bottleneck principle Tishby & Zaslavsky (2015) to learn a minimal sufficient subgraph for GNN explainability, which is shown to be generalizable under distribution shifts. OOD-GNN Li et al. (2022a) proposes to learn disentangled graph representation by computing global weights of all data. Parallel to all previous studies, we propose ELiSD, which utilizes spurious subgraph diversification to provably identify G_c for OOD generalization, and uplift the lower bound of $I(G;Y)$ to enhance feature learning simultaneously. In this study, we adopt the same learning paradigm as EQuAD, and we propose instance-level adaptive biased infomax and intra-class cross entropy loss to enhance the efficacy of learning spurious and invariant features respectively.

Node-Level OOD Generalization. There has also been a substantial amount of work focusing on the OOD generalization problem on node-level classification tasks. Most of these studies (Wu et al., 2022a; Liu et al., 2023; Li et al., 2023a; Yu et al., 2023) also focus on environment generation, which facilitates the subsequent invariant learning. These methods are also likely to learn only a subset of invariant features, thus limiting their ability to generalize to OOD data.

GNN Explainability. GNN explanation methods can be broadly categorized into instance-level (Luo et al., 2020; Ying et al., 2019; Pope et al., 2019; Schnake et al., 2021) and model-level (Azzolin et al., 2022; Yuan et al., 2020; Wang & Shen, 2022) explanations. The main goal of the instance-level explanation methods is to explain why a certain prediction is made for a particular instance. Specifically, the important input subgraph and features that contribute the most to model predictions are identified for a given instance. In this work, we employ instance-level GNN explanation methods to approximate the invariant subgraph G_c, and utilize off-the-shelf method GSAT (Miao et al., 2022), that is robust under distribution shifts, to identify the important nodes in a graph to facilitate the learning of graph spuriosity through adaptive biased infomax in real-world datasets.

D THEORETICAL RESULTS

D.1 THEORETICAL DISCUSSION ON VREX IN LEARNING INVARIANT FEATURES

We first outline the objective function of VRex as following:

$$\mathcal{L}_{VRex} := \min_{w,\phi} \mathbb{E}_e \left[\mathcal{L}\left(w \circ \phi\left(X\right), Y\right)\right] + \beta \operatorname{Var}_e \left[\mathcal{L}\left(w \circ \phi\left(X\right), Y\right)\right], \tag{10}$$

here w and ϕ denote the classifier and feature extractor, respectively. β is the hyperparameter to control regularization strength. Next we prove the following proposition.

Proposition 3. *Let $w^*, \phi^* = \underset{w,\phi}{\operatorname{argmin}} \mathcal{L}_{VRex}$, then $\widehat{\mathbf{h}}_G = w^*(X)$ learns invariant features, however $\widehat{\mathbf{h}}_G$ may only contain a subset of invariant features, given our PIIF data generating assumption:*

$$Y = X_c + n_1, X_s = Y + n_2 + \epsilon^e, \text{ where } X_c := \sum_i X_{c,i}, X_s := \sum_i X_{s,i}, \tag{11}$$

and FIIF data generating assumption:

$$Y = X_c + n_1, X_s = n_2 + \epsilon^e, \text{ where } X_c := \sum_i X_{c,i}, X_s := \sum_i X_{s,i}, \tag{12}$$

when using a linear classifier $\phi(X) = w_1 X_c + w_2 X_s$, and $\mathcal{L}(w \circ \phi(X)) := R(e) = (\phi(X) - Y)^2$.

Here, we assume an additive model for X_c, i.e., A set of invariant features $X_{c,i}$ is combined through summation to obtain the final X_c, and similarly for X_s.

Proof. To prove Prop. 3, we first expand $\operatorname{Var}_e(R(e)) = \mathbb{E}_e\left[R^2(e)\right] - \left(\mathbb{E}_e[R(e)]\right)^2$, then we take derivative w.r.t. w_1 and w_2, we then show that Eqn. 10 can elicit w^* that learns invariant features, however, it may only learn a subset of them.

Given $R(e) = (\phi(X) - Y)^2$ and $\operatorname{Var}_e(R(e)) = \mathbb{E}_e R^2(e) - \mathbb{E}_e^2 R(e)$, we have:

$$\begin{aligned} \frac{\partial \operatorname{Var}_e(R(e))}{\partial w_1} &= \frac{\partial \mathbb{E}_e[(\phi(X) - Y)^4]}{\partial w_1} - \mathbb{E}_e^2[(\phi(X) - Y)^2] \\ &= 4\mathbb{E}_e[(\phi(X) - Y)^3 X_c] - 4\mathbb{E}_e[R(e)] \cdot \mathbb{E}_e[(\phi(X) - Y) X_c]. \end{aligned} \tag{13}$$

Similarly, for $\frac{\partial \operatorname{Var}_e(R(e))}{\partial w_2}$, we have:

$$\frac{\partial \operatorname{Var}_e(R(e))}{\partial w_2} = 4E_e\left[(\phi(X) - Y)^3 \cdot (X_c + n_1 + n_2 + \varepsilon^e)\right] - 4E_e[R(e)] \cdot E_e\left[(\phi(X) - Y) \cdot (X_c + n_1 + n_2 + \epsilon^e)\right]. \tag{14}$$

Now we expand $\phi(X) - Y$:

$$\begin{gathered} \phi(X) = w_1 X_c + w_2 X_s \\ X_s = X_c + n_1 + n_2 + \varepsilon^e \\ \phi(X) = (w_1 + w_2) X_c + w_2 n_1 + w_2 n_2 + w_2 \varepsilon^e \\ Y = X_c + n_1 \\ \phi(X) - Y = (w_1 + w_2 - 1) X_c + (w_2 - 1) n_1 + w_2 n_2 + w_2 \varepsilon^e \end{gathered} \tag{15}$$

Next, we show that $w_1 = 1, w_2 = 0$ is a optimal solution for minimizing Eqn. 10. We set $w_1 = 1, w_2 = 0$, and plug into $\phi(X)$ and $\phi(X) - Y$, we get:

$$\phi(X) = w_1 X_c + w_2 X_s \rightarrow \phi(X) = 1 \cdot X_c + 0 \cdot X_s = X_c, \tag{16}$$

and

$$\begin{aligned} Y &= X_c + n_1 \\ \phi(X) - Y &= X_c - (X_c + n_1) = -n_1. \end{aligned} \tag{17}$$

Substitute Eqn. 1617 into Eqn. 13, we get:

$$\begin{aligned} 4\mathbb{E}_e\left[(\phi(X) - Y)^3 \cdot X_c\right] = 4\mathbb{E}_e\left[\mathbb{E}_{n_1,n_2}\ \left[(-n_1)^3 \cdot X_c\right]\right] = 0 \qquad (E_e[n_1^3] = 0) \\ E_e[R(e)] = E_e\left[n_1^2\right] = \sigma_{n1}^2 \\ \mathbb{E}_e\left[\mathbb{E}_{n_1,n_2}\left[(-n_1) \cdot X_c\right]\right] = 0, \end{aligned} \tag{18}$$

therefore, we have $\frac{\partial \operatorname{Var}_e(R(e))}{\partial w_1} = 0$. For $\frac{\partial \operatorname{Var}_e(R(e))}{\partial w_2}$ (Eqn. 14), the first term can be expanded as:

$$\begin{aligned} \mathbb{E}_e\left[(-n_1)^3 \cdot X_c\right] = 0 \\ \mathbb{E}_e\left[\mathbb{E}_{n_1,n_2}\left[(-n_1)^3 \cdot n_1\right]\right] = -\mathbb{E}_e\left[\mathbb{E}_{n_1,n_2}\left[n_1^4\right]\right] = -3\sigma_{n1}^4 \\ \mathbb{E}_e\left[\mathbb{E}_{n_1,n_2}\left[(-n_1)^3 \cdot n_2\right]\right] = 0 \\ \mathbb{E}_e\left[\mathbb{E}_{n_1,n_2}\left[(-n_1)^3 \cdot \varepsilon^e\right]\right] = 0, \end{aligned} \tag{19}$$

thus:

$$4\mathbb{E}_e\left[\mathbb{E}_{n_1,n_2}\left[(-n_1)^3 \cdot (X_c + n_1 + n_2 + \varepsilon^e)\right]\right] = 4 \cdot \left(-3\sigma_{n1}^4\right) = -12\sigma_{n1}^4. \tag{20}$$

For the second term in Eqn. 14:

$$4\mathbb{E}_e[R(e)] \cdot \mathbb{E}_e\left[\mathbb{E}_{n_1,n_2}\left[(-n_1) \cdot (X_c + n_1 + n_2 + \varepsilon^e)\right]\right] = 4\sigma_{n1}^2 \cdot \left(-\sigma_{n1}^2\right) = -4\sigma_{n1}^4, \tag{21}$$

substitute Eqn. 20 and 21 into Eqn. 14, we get:

$$\frac{\partial \operatorname{Var}_e(R(e))}{\partial w_2} = -8\sigma_{n1}^4. \tag{22}$$

As σ_{n1} is the standard deviation of n_1, where X_c is causally related with Y, we assume σ_{n1} is a small value, hence the high-order term $\mathcal{O}(\sigma_{n1}^4) \approx 0$. Therefore, we show that $w_1 = 1, w_2 = 0$ is (approxiamately) optimla solution for Eqn. 10, indicating that only the invariant features are used in the classifier $\phi^*(X)$. Now we have:

$$Y = \phi^*(X) = X_c = \sum_i X_{c,i}. \tag{23}$$

Given a fixed value $X_c = x$, there may be multiple combinations for $\{X_{c,i}\}$ that result in $X_c = x$. The set of invariant features $\{X_{c,i}\}$ naturally arises from the learning process of deep neural networks. Some invariant features might be easier to learn due to their salience or higher frequency in the dataset. Consequently, although the VRex objective promotes the learning of invariant encoders (as we have proved above), it does not guarantee the identification of all invariant features $\{X_{c,i}\}$.

For FIIF data generating process, similarly we get:

$$\begin{aligned} \phi(X) = w_1 X_c + w_2 X_s, \quad X_s = n_2 + \epsilon^e, \quad Y = X_c + n_1, \Rightarrow \\ \phi(X) - Y = (w_1 - 1)X_c + w_2 n_2 + w_2 \epsilon^e - n_1. \end{aligned} \tag{24}$$

The variance of the loss across environments is:

$$\mathrm{Var}_e\left[(\phi(X)-Y)^2\right]=\mathbb{E}_e\left[(\phi(X)-Y)^4\right]-\left(\mathbb{E}_e\left[(\phi(X)-Y)^2\right]\right)^2. \tag{25}$$

Recall that $\phi(X)=w_1X_c+w_2X_s$ and $X_s=n_2+\epsilon^e$, we have:

$$\phi(X)-Y=(w_1-1)\,X_c+w_2n_2+w_2\epsilon^e-n_1. \tag{26}$$

The squared expected loss term can be expanded as:

$$\begin{aligned}\mathbb{E}_e\left[(\phi(X)-Y)^2\right]&=\mathbb{E}_e\left[\left((w_1-1)\,X_c+w_2n_2+w_2\epsilon^e-n_1\right)^2\right]\\&=(w_1-1)^2\,\mathbb{E}_e\left[X_c^2\right]+w_2^2\mathbb{E}_e\left[n_2^2\right]\\&\quad+w_2^2\mathbb{E}_e\left[\left(\epsilon^e\right)^2\right]+\mathbb{E}_e\left[n_1^2\right]\\&\quad+2\,(w_1-1)\,w_2\mathbb{E}_e\left[X_cn_2\right].\end{aligned} \tag{27}$$

Given the independence between X_c, n_1, n_2 and ϵ^e, we have:

$$\mathbb{E}_e\left[(\phi(X)-Y)^2\right]=(w_1-1)^2\,\mathbb{E}_e\left[X_c^2\right]+w_2^2\mathbb{E}_e\left[n_2^2\right]+w_2^2\mathbb{E}_e\left[\left(\epsilon^e\right)^2\right]+\mathbb{E}_e\left[n_1^2\right] \tag{28}$$

For $\mathbb{E}_e\left[(\phi(X)-Y)^4\right]$, we have:

$$\begin{aligned}\mathbb{E}_e\left[(\phi(X)-Y)^4\right]&=\mathbb{E}_e\left[\left((w_1-1)\,X_c+w_2n_2+w_2\epsilon^e-n_1\right)^4\right]\\&=(w_1-1)^4\,\mathbb{E}_e\left[X_c^4\right]+w_2^4\mathbb{E}_e\left[n_2^4\right]\\&\quad+w_2^4\mathbb{E}_e\left[\left(\epsilon^e\right)^4\right]+\mathbb{E}_e\left[n_1^4\right].\end{aligned} \tag{29}$$

Taking derivative with respect to w_1 and w_2:

$$\begin{aligned}\frac{\partial}{\partial w_1}\mathbb{E}_e\left[(\phi(X)-Y)^2\right]&=2\,(w_1-1)\,\mathbb{E}_e\left[X_c^2\right],\\\frac{\partial}{\partial w_1}\mathbb{E}_e\left[(\phi(X)-Y)^4\right]&=4\,(w_1-1)^3\,\mathbb{E}_e\left[X_c^4\right],\\\frac{\partial}{\partial w_2}\mathbb{E}_e\left[(\phi(X)-Y)^2\right]&=2w_2\left(\mathbb{E}_e\left[n_2^2\right]+\mathbb{E}_e\left[\left(\epsilon^e\right)^2\right]\right),\\\frac{\partial}{\partial w_2}\mathbb{E}_e\left[(\phi(X)-Y)^4\right]&=4w_2^3\left(\mathbb{E}_e\left[n_2^4\right]+\mathbb{E}_e\left[\left(\epsilon^e\right)^4\right]\right).\end{aligned} \tag{30}$$

Setting Eqn. 30 to zero, we get $w_1=1, w_2=0$. In conclusion, for both PIIF and FIIF data generating scenarios, VRex only learns invariant features, however given an additive model, it may only learn a subset of invariant features that are significant or frequently appears in the training set.

□

D.2 Theoretical Discussion on IRMv1 in Learning Invariant Features

Using a similar derivation process, we can prove that IRMv1 may only learn a subset of invariant features. We first outline the objective of IRMv1 as follows:

$$\mathcal{L}_{IRMv1}:=\min_{w,\phi}\mathbb{E}_e\left[\mathcal{L}\left(w\circ\phi\left(X\right),Y\right)+\beta\left\|\nabla_{w|w=1.0}\mathcal{L}\left(w\circ\phi\left(X\right),Y\right)\right\|_2^2\right], \tag{31}$$

here w and ϕ denote the classifier and feature extractor, respectively.

Proposition 4. *Let* $w^*, \phi^* = \underset{w,\phi}{\text{argmin}} \mathcal{L}_{IRMv1}$*, then* $\widehat{\mathbf{h}}_G = w^*(X)$ *learns invariant features, however* $\widehat{\mathbf{h}}_G$ *may only contain a subset of invariant features, given our data generating assumption:*

$$Y = X_c + n_1, X_s = Y + n_2 + \epsilon^e, \text{ where } X_c := \sum_i X_{c,i}, X_s := \sum_i X_{s,i}, \tag{32}$$

and FIIF data generating assumption:

$$Y = X_c + n_1, X_s = n_2 + \epsilon^e, \text{ where } X_c := \sum_i X_{c,i}, X_s := \sum_i X_{s,i}, \tag{33}$$

when using a linear classifier $\phi(X) = w_1 X_c + w_2 X_s$*, and* $\mathcal{L}(w \circ \phi(X)) := R(e) = (\phi(X) - Y)^2$*.*

Proof. The IRMv1 objective can be simplied into:

$$\mathcal{L}_{IRMv1} := \left\| \nabla_{w|w=1.0} \mathcal{L}(w \circ \phi(X), Y) \right\|_2^2 = (\phi(X) - Y)^4, \tag{34}$$

given:

$$\begin{aligned} \phi(X) &= w_1 X_c + w_2 X_s \\ X_s &= X_c + n_1 + n_2 + \varepsilon^e \\ Y &= X_c + n_1, \end{aligned} \tag{35}$$

we get:

$$\begin{aligned} \phi(X) = w_1 X_c + w_2 \left(X_c + n_1 + n_2 + \varepsilon^e\right) &= \left(w_1 + w_2\right) X_c + w_2 n_1 + w_2 n_2 + w_2 \varepsilon^e \\ \phi(X) - Y &= \left(w_1 + w_2 - 1\right) X_c + \left(w_2 - 1\right) n_1 + w_2 n_2 + w_2 \varepsilon^\varepsilon. \end{aligned} \tag{36}$$

Taking gradient w.r.t. w_1 and w_2 respetively:

$$\begin{aligned} \frac{\partial (\phi(X) - Y)^4}{\partial w_1} &= 4(\phi(X) - Y)^3 \cdot \frac{\partial (\phi(X) - Y)}{\partial w_1} \\ &= 4(\phi(X) - Y)^3 \cdot X_c, \end{aligned} \tag{37}$$

and

$$\begin{aligned} \frac{\partial (\phi(X) - Y)^4}{\partial w_2} &= 4(\phi(X) - Y)^3 \cdot \frac{\partial (\phi(X) - Y)}{\partial w_2} \\ &= 4(\phi(X) - Y)^3 \cdot \left(X_c + n_1 + n_2 + \varepsilon^e\right). \end{aligned} \tag{38}$$

Plugging in $w_1 = 1, w_2 = 0$, we get:

$$\begin{aligned} \phi(X) &= X_c \\ \phi(X) - Y &= -n_1, \end{aligned} \tag{39}$$

Substitue Eqn. 39 into Eqn. 37 and Eqn. 38, we get:

$$\mathbb{E}_e \left[\frac{\partial (\phi(X) - Y)^4}{\partial w_1} \right] = \mathbb{E}_e \left[\mathbb{E}_{n_1, n_2} \left[-4 n_1^3 \cdot X_c \right] \right] = 0, \tag{40}$$

and

$$\mathbb{E}_e\left[\frac{\partial(\phi(X)-Y)^4}{\partial w_2}\right] = \mathbb{E}_e\left[-4n_1^3\cdot(X_c+n_1+n_2+\varepsilon^e)\right]$$
$$= -4\mathbb{E}_e\mathbb{E}_{n_1,n_2}\left[n_1^3\cdot X_c\right] - 4\mathbb{E}_e\mathbb{E}_{n_1,n_2}\left[n_1^3\cdot n_1\right] - 4\mathbb{E}_e\mathbb{E}_{n_1,n_2}\left[n_1^3\cdot n_2\right] - 4\mathbb{E}_e\mathbb{E}_{n_1,n_2}\left[n_1^3\cdot \varepsilon^e\right], \tag{41}$$

given that:

$$\begin{aligned}\mathbb{E}_{n_1,n_2}\left[n_1^3\cdot X_c\right] &= 0\\ \mathbb{E}_{n_1,n_2}\left[n_1^3\cdot n_1\right] &= \mathbb{E}_{n_1,n_2}\left[n_1^4\right] = 3\sigma_{n1}^4\\ \mathbb{E}_{n_1,n_2}\left[n_1^3\cdot n_2\right] &= 0\\ \mathbb{E}_{n_1,n_2}\left[n_1^3\cdot \varepsilon^e\right] &= 0,\end{aligned} \tag{42}$$

we have $\mathbb{E}_e\left[\frac{\partial(\phi(X)-Y)^4}{\partial w_2}\right] = -12\sigma_{n1}^4$, with a similar assumption that the standard error σ_{n1} of the Gaussian noise n_1 of the causal variable X_c is small, we conclude that $\mathbb{E}_e\left[\frac{\partial(\phi(X)-Y)^4}{\partial w_2}\right] = \mathcal{O}(\sigma_{n1}^4) \approx 0$. Hence IRMv1 learns invariant features under the data generating process. Now we have:

$$Y = \phi^*(X) = X_c = \sum_i X_{c,i}. \tag{43}$$

For FIIF generating process, applying the same technique, we have:

$$\begin{aligned}\phi(X)-Y = w_1X_c + w_2\left(n_2+\epsilon^e\right) - \left(X_c+n_1\right) = \left(w_1-1\right)X_c + w_2n_2 + w_2\epsilon^e - n_1.\\ \frac{\partial\mathcal{L}_{IRMv1}}{\partial w_1} = 4(\phi(X)-Y)^3\cdot\frac{\partial}{\partial w_1}(\phi(X)-Y).\\ \frac{\partial}{\partial w_1}(\phi(X)-Y) = X_c.\end{aligned} \tag{44}$$

Therefore:

$$\begin{aligned}\frac{\partial\mathcal{L}_{IRMv1}}{\partial w_1} &= 4(\phi(X)-Y)^3\cdot X_c = 4\left(\left(w_1-1\right)X_c + w_2n_2 + w_2\epsilon^e - n_1\right)^3 X_c.\\ \frac{\partial\mathcal{L}_{IRMv1}}{\partial w_2} &= 4(\phi(X)-Y)^3\cdot\frac{\partial}{\partial w_2}(\phi(X)-Y) = 4(\phi(X)-Y)^3\cdot(n_2+\epsilon^e)\end{aligned} \tag{45}$$

Substitute $w_1 = 1, w_2 = 0$ into $\phi(X) - Y$,:

$$\phi(X) - Y = X_c - (X_c + n_1) = -n_1. \tag{46}$$

Taking derivative w.r.t. w_1 and w_2:

$$\mathbb{E}_e\left[\frac{\partial\mathcal{L}_{IRMv1}}{\partial w_1}\right] = -4\mathbb{E}_e\left[n_1^3X_c\right] = 0, \tag{47}$$

$$\mathbb{E}_e\left[\frac{\partial\mathcal{L}_{IRMv1}}{\partial w_2}\right] = 4\mathbb{E}_e\left[n_1^3\left(n_2+\epsilon^e\right)\right] = 0. \tag{48}$$

Therefore we show that for the widely used FIIF and PIIF data generating process, IRMv1 is able to learn invariant features. However, with a similar reasoning as VRex, there may be multiple combinations of the assignments for $\{X_{c,i}\}$ to lead to a fixed value $X_c = x$, and the objective of IRMv1 (Eqn. 31) won't ensure the learning of all invariant features.

□

D.3 PROOF OF THEOREM 4.1

Theorem D.1. *[Restatement of Theorem 4.1] Given that the invariant subgraph G_c contains invariant patterns causally related to the target labels, and G_s contains only spurious patterns, the biased infomax principle achieves spuriosity learning. Specifically, the encoder $h_\theta(\cdot)$ learns solely the spurious features for each data sample in $\mathcal{D}$.*

We begin by stating the assumption underlying our proof, followed by a proof by contradiction.

Assumption 2. (*Existence of spuriosity learner*) There exists a learning algorithm capable of achieving spuriosity learning as defined in Def. 2.

Most invariant learning algorithms aim to learn invariant features, and a large collection of literature has demonstrated the existence of such algorithms (Arjovsky et al., 2020; Kreuzer et al., 2021; Parascandolo et al., 2020; Mahajan et al., 2021; Wald et al., 2021; Ahuja et al., 2020; 2021; Chen et al., 2022; Gui et al., 2023; Liu et al., 2022). In contrast, we assume the existence of algorithms that learn spurious features. One such example is provided by Eastwood et al. (2023), where the method learns both invariant and spurious features, supporting the plausibility of our assumption. Recent studies have shown that self-supervised contrastive learning tends to learn spurious features (Yao et al., 2024; Hamidieh et al., 2024; Meehan et al., 2023). Therefore, self-supervised contrastive learning would be one form of the spuriosity learner. Based on the above, we first sketch our proof.

Proof sketch. As biased infomax is a more general form of the infomax principle, with exponentially many *node configurations* (Def. 4), the encoder $h_{\theta'}(\cdot)$ under the optimal node configuration must result in a spuriosity learner, which also maximizes the learning objective. We then employ proof by contradiction to demonstrate that the node configuration corresponding to biased infomax in Def 3 leads to a larger mutual information, thereby eliciting a contradiction, leading to the conclusion that the *node configuration* corresponding to Def 3 elicits the spuriosity learner.

Definition 4. (*Node configurations*) Let the general form of biased infomax be:

$$\begin{aligned} &\max_\theta \mathbb{E}_{G\sim\mathcal{G}} \frac{1}{|G|}\left(\sum_{v_i\in\widetilde{G}} I\left(\widehat{\mathbf{h}}_i;\widehat{\mathbf{h}}_G\right) - \sum_{v_i\in G\setminus\widetilde{G}} I\left(\widehat{\mathbf{h}}_i;\widehat{\mathbf{h}}_G\right)\right), \\ &\text{s.t. } \widehat{\mathbf{h}}_i = h_\theta(G), \widehat{\mathbf{h}}_G = \text{READOUT}\left(\widehat{\mathbf{h}}_i\right). \end{aligned} \tag{49}$$

A node configuration $\mathbf{c} = \left(c_1, c_2, \ldots, c_{|\mathcal{V}|}\right)^T$, such that $c_i \in \{-1, 1\}$, corresponds to one specific instantiation in Eqn. 49, where $c_i = 1$ denotes that $v_i \in \widetilde{G}$, and $c_i = -1$ means $v_i \in G \setminus \widetilde{G}$. The set of all possible node configurations can be denoted as $\mathcal{H} := \{\mathbf{c} : c_i \in \{-1, 1\}\}$.

Given definition 4, the infomax principle (Eqn. 1) is therefore a special case of the biased infomax principle, where $\mathbf{c} = \mathbf{1}_{|\mathcal{V}|}$. For notation simplicity, let $\mathbf{c} := [\mathbf{c}_1, \mathbf{c}_2]^T, \mathbf{c}_1 \in \mathbb{R}^{|G_s|}, \mathbf{c}_2 \in \mathbb{R}^{|G_c|}$ be two vectors for the node configurations of G_s and G_c. Assuming for the optimal node configuration, there are k elements in $\mathbf{c}_1$ with 1, and $|G_s| - k$ elements with -1 (denoted as $\mathcal{V}_s^{\mathbf{1}}$ and $\overline{\mathcal{V}_s^{\mathbf{1}}}$), similarly, there are t elements in $\mathbf{c}_2$ with 1, and $|G_c| - t$ elements with -1, denoted as $\mathcal{V}_c^{\mathbf{1}}$ and $\overline{\mathcal{V}_c^{\mathbf{1}}}$. We then compare such node configuration $\mathbf{c}^*$ with $\mathbf{c}' = [\mathbf{1}_{|G_s|}, -\mathbf{1}_{|G_c|}]^T$.

Proof. First, under the node configuration $\mathbf{c}^*$, the optimal parameter to optimize the learning objective is:

$$\theta^* = \arg\max_\theta \mathbb{E}_{G\sim\mathcal{G}} \frac{1}{|G|}\left(\sum_{v_i\in\mathcal{V}_s^{\mathbf{1}}} I\left(\widehat{\mathbf{h}}_i;\widehat{\mathbf{h}}_G\right) + \sum_{v_i\in\mathcal{V}_c^{\mathbf{1}}} I\left(\widehat{\mathbf{h}}_i;\widehat{\mathbf{h}}_G\right) - \sum_{v_i\in\overline{\mathcal{V}_s^{\mathbf{1}}}} I\left(\widehat{\mathbf{h}}_i;\widehat{\mathbf{h}}_G\right) - \sum_{v_i\in\overline{\mathcal{V}_c^{\mathbf{1}}}} I\left(\widehat{\mathbf{h}}_i;\widehat{\mathbf{h}}_G\right)\right), \tag{50}$$

and under the node configuration $\mathbf{c}'$, the optimal parameter is:

$$\theta' = \arg\max_{\theta} \mathbb{E}_{G\sim\mathcal{G}} \frac{1}{|G|} \left(\sum_{v_i \in G_s} I\left(\widehat{\mathbf{h}}_i; \widehat{\mathbf{h}}_G\right) - \sum_{v_i \in G_c} I\left(\widehat{\mathbf{h}}_i; \widehat{\mathbf{h}}_G\right) \right). \tag{51}$$

Let

$$f(\theta^*; \mathcal{D}, \mathbf{c}^*) := \mathbb{E}_{G\sim\mathcal{G}} \frac{1}{|G|} \left(\sum_{v_i \in \mathcal{V}_s^{\mathbf{1}}} I\left(\widehat{\mathbf{h}}_i; \widehat{\mathbf{h}}_G\right) + \sum_{v_i \in \mathcal{V}_c^{\mathbf{1}}} I\left(\widehat{\mathbf{h}}_i; \widehat{\mathbf{h}}_G\right) - \sum_{v_i \in \overline{\mathcal{V}_s^{\mathbf{1}}}} I\left(\widehat{\mathbf{h}}_i; \widehat{\mathbf{h}}_G\right) - \sum_{v_i \in \overline{\mathcal{V}_c^{\mathbf{1}}}} I\left(\widehat{\mathbf{h}}_i; \widehat{\mathbf{h}}_G\right) \right)$$

. Similarly, we can define

$$f(\theta'; \mathcal{D}, \mathbf{c}') := \mathbb{E}_{G\sim\mathcal{G}} \frac{1}{|G|} \left(\sum_{v_i \in G_s} I\left(\widehat{\mathbf{h}}_i; \widehat{\mathbf{h}}_G\right) - \sum_{v_i \in G_c} I\left(\widehat{\mathbf{h}}_i; \widehat{\mathbf{h}}_G\right) \right)$$

.

According to Eqn. 51, we can conclude that $f(\theta'; \mathcal{D}, \mathbf{c}') > f(\theta^*; \mathcal{D}, \mathbf{c}')$, and we also have that $h_{\theta^*}(\cdot) = \widehat{\mathbf{h}}_G$ only learns spurious features as θ^* is the maximizer for the objective under $\mathbf{c}^*$, and $h_{\theta'}(\cdot) = \widehat{\mathbf{h}}_G$ learns both invariant and spurious features, as θ' is the maximizer for the objective under $\mathbf{c}'$. Let $\mathbf{h}_G^{\theta^*} = h_{\theta^*}(G)$, and $\mathbf{h}_G^{\theta'} = h_{\theta'}(G)$, therefore we have:

$$I\left(\widehat{\mathbf{h}}_i; \widehat{\mathbf{h}}_G^{\theta^*}\right) = 0, \quad \forall v_i \in G_c; \tag{52}$$

$$I\left(\widehat{\mathbf{h}}_i; \widehat{\mathbf{h}}_G^{\theta'}\right) = c, \quad \forall v_i \in G_c; \tag{53}$$

$$I\left(\widehat{\mathbf{h}}_i; \widehat{\mathbf{h}}_G^{\theta^*}\right) = q, \quad \forall v_i \in G_s; \tag{54}$$

$$I\left(\widehat{\mathbf{h}}_i; \widehat{\mathbf{h}}_G^{\theta'}\right) = q', \quad \forall v_i \in G_s; \tag{55}$$

Eqn. 52 is due to $h_{\theta^*}(\cdot)$ is obtained under $\mathbf{c}^*$, hence only learn spuriosity. Eqn. 53 is due to that $h_{\theta'}(\cdot)$ learns both spurious and invariant features. We also have $q > q'$ due to the same reason. Now we compare $f(\theta'; \mathcal{D}, \mathbf{c}')$ with $f(\theta^*; \mathcal{D}, \mathbf{c}')$ as follows:

$$\begin{aligned} f\left(\theta^*; \mathcal{D}, \mathbf{c}'\right) - f\left(\theta'; \mathcal{D}, \mathbf{c}'\right) &= \mathbb{E}_{G\sim\mathcal{G}} \frac{1}{|G|} \left(\sum_{v_i \in G_s} q - \sum_{v_i \in G_c} 0 \right) \\ &\quad - \left(\mathbb{E}_{G\sim\mathcal{G}} \frac{1}{|G|} \left(|G_s| \cdot q' - |G_c| \cdot c\right) \right) \\ &= \mathbb{E}_{G\sim\mathcal{G}} \frac{1}{|G|} \left(|G_s|(q - q') + |G_c| \cdot c\right) > 0, \end{aligned} \tag{56}$$

leading to a contradiction that $f(\theta'; \mathcal{D}, \mathbf{c}') > f(\theta^*; \mathcal{D}, \mathbf{c}')$ for any node configuration $\mathbf{c} \neq \mathbf{c}'$, therefore we conclude that $\mathbf{c}'$ is the optimal configuration that elicits the spuriosity learner, which corresponds to the biased infomax objective in Eqn. 2.

□

D.4 Proof of Proposition 1

Proposition 5. *[Restatement of Proposition 1] Given an error rate $p\%$ in the approximation algorithm for G_c, let the learning objectives for the biased infomax with the ground-truth subgraphs G_c and G_s and with the approximated subgraphs $\widehat{G}_c$ and $\widehat{G}_s$ be denoted as $\mathcal{L}(\theta^*; \mathcal{D})$ and $\mathcal{L}(\theta'; \mathcal{D})$ respectively. The difference between $\mathcal{L}(\theta^*; \mathcal{D})$ and $\mathcal{L}(\theta'; \mathcal{D})$ can be expressed as:*

$$\mathbb{E}_{G\sim\mathcal{G}} \left[\frac{2}{|G|} \left(\sum_{v_i \in pG_s} I\left(\widehat{\mathbf{h}}_i; \widehat{\mathbf{h}}_G\right) - \sum_{v_i \in pG_c} I\left(\widehat{\mathbf{h}}_i; \widehat{\mathbf{h}}_G\right) \right) \right].$$

Proof. We first expand $\mathcal{L}(\theta^*;\mathcal{D})$ and $\mathcal{L}(\theta';\mathcal{D})$ as follows.

$$\begin{aligned}\mathcal{L}(\theta^*;\mathcal{D}) &= \mathbb{E}_{G\sim\mathcal{G}}\frac{1}{|G|}\left(\sum_{v_i\in G_s} I\left(\widehat{\mathbf{h}}_i;\widehat{\mathbf{h}}_G\right) - \sum_{v_i\in G_c} I\left(\widehat{\mathbf{h}}_i;\widehat{\mathbf{h}}_G\right)\right)\\ &= \mathbb{E}_{G\sim\mathcal{G}}\frac{1}{|G|}\left(\sum_{v_i\in(1-p)G_s} I\left(\widehat{\mathbf{h}}_i;\widehat{\mathbf{h}}_G\right) + \sum_{v_i\in pG_s} I\left(\widehat{\mathbf{h}}_i;\widehat{\mathbf{h}}_G\right) - \sum_{v_i\in(1-p)G_c} I\left(\widehat{\mathbf{h}}_i;\widehat{\mathbf{h}}_G\right) - \sum_{v_i\in pG_c} I\left(\widehat{\mathbf{h}}_i;\widehat{\mathbf{h}}_G\right)\right)\end{aligned}$$

and

$$\mathcal{L}(\theta';\mathcal{D}) = \mathbb{E}_{G\sim\mathcal{G}}\frac{1}{|G|}\left(\sum_{v_i\in(1-p)G_s\cup pG_c} I\left(\widehat{\mathbf{h}}_i;\widehat{\mathbf{h}}_G\right) - \sum_{v_i\in(1-p)G_c\cup pG_s} I\left(\widehat{\mathbf{h}}_i;\widehat{\mathbf{h}}_G\right)\right). \tag{57}$$

the gap of the two learning objectives $\Delta\mathcal{L}$ is:

$$\begin{aligned}\Delta\mathcal{L} &:= \mathcal{L}(\theta^*;\mathcal{D}) - \mathcal{L}(\theta';\mathcal{D})\\ &= \mathbb{E}_{G\sim\mathcal{G}}\frac{1}{|G|}\left(\sum_{v_i\in(1-p)G_s} I\left(\widehat{\mathbf{h}}_i;\widehat{\mathbf{h}}_G\right) + \sum_{v_i\in pG_s} I\left(\widehat{\mathbf{h}}_i;\widehat{\mathbf{h}}_G\right) - \sum_{v_i\in(1-p)G_c} I\left(\widehat{\mathbf{h}}_i;\widehat{\mathbf{h}}_G\right) - \sum_{v_i\in pG_c} I\left(\widehat{\mathbf{h}}_i;\widehat{\mathbf{h}}_G\right)\right)\\ &- \left(\mathbb{E}_{G\sim\mathcal{G}}\frac{1}{|G|}\left(\sum_{v_i\in(1-p)G_s\cup pG_c} I\left(\widehat{\mathbf{h}}_i;\widehat{\mathbf{h}}_G\right) - \sum_{v_i\in(1-p)G_c\cup pG_s} I\left(\widehat{\mathbf{h}}_i;\widehat{\mathbf{h}}_G\right)\right)\right).\\ &= \mathbb{E}_{G\sim\mathcal{G}}\frac{2}{|G|}\left[\sum_{v_i\in pG_s} I\left(\widehat{\mathbf{h}}_i;\widehat{\mathbf{h}}_G\right) - \sum_{v_i\in pG_c} I\left(\widehat{\mathbf{h}}_i;\widehat{\mathbf{h}}_G\right)\right].\end{aligned} \tag{58}$$

We conclude the proof.

□

D.5 Proof of Proposition 2

Proposition 6. *[Restatement of Proposition 2] Given a linear regression model with parameters $\{\theta_1,\theta_2\}$ and spurious features $\{x_1,x_2\}$, the correlation strength for feature x_1 is p and for x_2 is $1-p$ when $Y=0$. Similarly, the correlation strength for feature x_1 is q and for x_2 is $1-q$ when $Y=1$. Assuming the spurious features x_1 and x_2 can each take values in $\{0,1\}$, we obtain the following parameter estimates using Mean Squared Error (MSE) loss: $\theta_1=\frac{q}{p+q}, \theta_2=\frac{1-q}{2-p-q}$.*

Proof. The linear model for predicting Y is: $\hat{Y}=\theta_1x_1+\theta_2x_2$, with Mean Square Error (MSE) loss, for $Y=0$ with pn samples, $x_1=1$ and $x_2=0$; with $(1-p)n$ samples, $x_1=0, x_2=1$; For $Y=1$ with qn samples, $x_1=1, x_2=0$, with $(1-q)n$ samples, $x_1=0, x_2=1$. The MSE loss $\mathcal{L}_{MSE}$ consists of 4 terms:

$$\begin{aligned}\mathcal{L}_{MSE} &= \sum_{i=1}^{pn}(\theta_1-0)^2 + \sum_{i=1}^{(1-p)n}(\theta_2-0)^2 + \sum_{i=1}^{qn}(\theta_1-1)^2 + \sum_{i=1}^{(1-q)n}(\theta_2-1)^2\\ &= pn\cdot\theta_1^2 + (1-p)n\cdot\theta_2^2 + qn\cdot(\theta_1-1)^2 + (1-q)n\cdot(\theta_2-1)^2\\ &= \frac{1}{4}\left[p\theta_1^2 + (1-p)\theta_2^2 + q\left(\theta_1-1\right)^2 + (1-q)\left(\theta_2-1\right)^2\right].\end{aligned}$$

Taking partial derivative w.r.t. θ_1:

$$\begin{aligned}\frac{\partial \mathcal{L}_{MSE}}{\partial \theta_1} &= \frac{1}{4}\left[2p\theta_1 + 2q\left(\theta_1 - 1\right)\right] = 0 \\ &\Rightarrow p\theta_1 + q\theta_1 - q = 0 \\ &\Rightarrow \theta_1 = \frac{q}{p+q}\end{aligned}$$

Similarly for θ_2,

$$\begin{aligned}\frac{\partial \mathcal{L}_{MSE}}{\partial \theta_2} &= \frac{1}{4}\left[2(1-p)\theta_2 + 2(1-q)\left(\theta_2 - 1\right)\right] = 0 \\ &\Rightarrow (1-p)\theta_2 + (1-q)\theta_2 - (1-q) = 0 \\ &\Rightarrow (2-p-q)\theta_2 = 1-q \\ &\Rightarrow \theta_2 = \frac{1-q}{2-p-q}\end{aligned}$$

□

As demonstrated in Proposition 2, the presence of spurious feature overlap across different classes hinders the linear classifier's ability to generate distinguishable (symmetric) logits. For instance, when $p = q$, both $\theta_1 = 0.5$ and $\theta_2 = 0.5$, resulting in a loss of distinguishability among different spurious patterns. To mitigate this issue, we propose class-conditioned (intra-class) cross entropy loss which reduces the interference across different classes. To show that class-conditioned (intra-class) cross entropy loss is able to maximize the conditional entropy $H(\mathbf{s}^{(i)}|\widehat{\mathbf{h}}_G^{(i)})$, we propose the following proposition.

Proposition 7. *Given the spurious features $\mathbf{h}_s^{(i)}, \forall G^{(i)} \in \mathcal{D}$ and a suitable clustering number K that corresponds to the number of environmental groups in each class $Y = y$, the loss objective $\mathcal{L}_{Inv}$ (Eqn. 3) will maximize the conditional entropy $H(\mathbf{s}^{(i)}|\widehat{\mathbf{h}}_G^{(i)}), \forall i \in \mathcal{D}$.*

To prove that optimizing $\mathcal{L}_{Inv}$ maximizes the conditional entropy $H(\mathbf{s}^{(i)}|\widehat{\mathbf{h}}_G^{(i)})$, we show that $\mathbb{P}(\mathbf{s}^{(i)}|\widehat{\mathbf{h}}_c^{(i)}) \sim Cat(\frac{1}{K})$ with K clusters, hence maximizes $H(\mathbf{s}^{(i)}|\widehat{\mathbf{h}}_G^{(i)})$.

Proof. First, we have:

$$\max_{\theta} H(\mathbf{s}^{(i)}|\widehat{\mathbf{h}}_G^{(i)}) = H(\mathbf{s}^{(i)}|\rho'(\widehat{\mathbf{h}}_G^{(i)})) = H(\mathbf{s}^{(i)}|\widehat{\mathbf{s}}^{(i)}). \tag{59}$$

Here, $\rho'(\cdot)$ is the classification head for cluster labels $\mathbf{s}^{(i)}$. For notation simplicity, we will omit superscript (i), and denote $\mathbf{s} := \mathbf{s}^{(i)}$ and $\widehat{\mathbf{s}} := \widehat{\mathbf{s}}^{(i)}$. Now using softmax loss, we have:

$$L = -\sum_{j=1}^{K} \mathbf{s}_j \log\left(\sigma(\widehat{\mathbf{s}})_j\right), \text{ where } \sigma(\widehat{\mathbf{s}})_j = \frac{e^{\widehat{\mathbf{s}}_j}}{\sum_{k=1}^{K} e^{\widehat{\mathbf{s}}_k}} \tag{60}$$

$$\frac{\partial \sigma(\widehat{\mathbf{s}})_j}{\partial \widehat{\mathbf{s}}_i} = \sigma(\widehat{\mathbf{s}})_j \left(\delta_{ij} - \sigma(\widehat{\mathbf{s}})_i\right) \tag{61}$$

$$\frac{\partial L}{\partial \widehat{\mathbf{s}}_i} = -\sum_{j=1}^{K} \mathbf{s}_j \frac{\partial \log\left(\sigma(\widehat{\mathbf{s}})_j\right)}{\partial \widehat{\mathbf{s}}_i} \Rightarrow \tag{62}$$

$$\frac{\partial L}{\partial \widehat{\mathbf{s}}_i} = -\left(\mathbf{s}_i - \sigma(\widehat{\mathbf{s}})_i\right). \tag{63}$$

Taking expectation on both side of Eqn. 63, we get:

$$\mathbb{E}\left[\frac{\partial L}{\partial \widehat{\mathbf{s}}_i}\right] = \mathbb{E}\left[-\left(\mathbf{s}_i - \sigma(\widehat{\mathbf{s}})_i\right)\right] \Rightarrow \tag{64}$$

$$0 = -\left(\mathbb{E}\left[\mathbf{s}_i\right] - \mathbb{E}\left[\sigma(\widehat{\mathbf{s}})_i\right]\right) \Rightarrow \tag{65}$$

$$0 = -\left(\frac{1}{K} - \mathbb{E}\left[\sigma(\widehat{\mathbf{s}})_i\right]\right) \Rightarrow \tag{66}$$

$$\mathbb{E}\left[\sigma(\widehat{\mathbf{s}})_i\right] = \frac{1}{K} \tag{67}$$

Eqn. 66 is due to that $\mathbb{E}[\mathbf{s}_i] = \frac{1}{K}$, as each cluster derived from the spurious embedding represents a environmental group, and with appropriate reweighting within each cluster, the samples will be weighted equally across clusters, i.e., samples from majority group and minority group will be weighted equally. Given that this expectation holds over all training samples, one optimal solution for Eqn. 67 is: $\sigma(\widehat{\mathbf{s}})_i = \frac{1}{K}, \forall i \in [K]$ for K class labels. This aligns with the assumption that within each class, there exists a stable pattern G_c, and if the encoder is able to effectively capture invariant patterns G_c while discarding spurious correlations, $\sigma(\widehat{\mathbf{s}})_i$ will be a fixed and constant value. With this constraint, the solution $\sigma(\widehat{\mathbf{s}}^{(i)}) = \frac{1}{K}\mathbf{1}_K$ implies that the model learns invariant features. Furthermore, this stable solution maximizes the conditional entropy $H(\mathbf{s}^{(i)}|\widehat{\mathbf{h}}_G^{(i)})$, as $\sigma(\widehat{\mathbf{s}}^{(i)})$ is independent of $\mathbf{s}^{(i)}$.

Remark. While $\sigma(\widehat{\mathbf{s}}^{(i)}) = \frac{1}{K}\mathbf{1}_K$ is a sufficient condition to minimize $\mathcal{L}_{\text{inv}}$, there exists other solutions that exploit spurious features to achieve high training accuracy. To guide the model toward the stable solution that satisfies $H(\mathbf{s}^{(i)}|\widehat{\mathbf{h}}_G^{(i)})$, an explicit regularization term, such as $\|\sigma(\widehat{\mathbf{s}}^{(i)}) - \frac{1}{K}\mathbf{1}_K\|_2^2$, can be added to the objective in Eqn. 4. However, our empirical results show that such explicit regularization does not significantly affect performance. This may be attributed to the limited number of class labels and node features in graph-level OOD datasets, which inherently enforce $\sigma(\widehat{\mathbf{s}}^{(i)})$ to be similar across all training samples, facilitating convergence to the stable solution.

□

D.6 Proof of Theorem 4.2

Theorem D.2. *[Restatement of Theorem 4.2] There exists a suitable γ and clustering number K, such that minimizing the loss objective $\mathcal{L} = \mathcal{L}_{GT} + \lambda\mathcal{L}_{Inv}$ will lead to the optimal encoder $h^*(\cdot)$ which elicits invariant features for any graph G, i.e., $\widehat{\mathbf{h}}_G = h^*(G) = \mathbf{h}_c$.*

Proof. We aim to show that minimizing the objective $\mathcal{L}$ encourages the encoder $h^*(\cdot)$ to learn representations $\widehat{\mathbf{h}}_G$ that contain only invariant features $\mathbf{h}_c$. First, consider that under ERM, i.e., minimizing $\mathcal{L}_{GT}$ alone, the encoder $h(\cdot)$ learns both invariant and spurious features, given the empirical and theoretical evidence in previous studies (Kirichenko et al., 2023; Chen et al., 2023b). Now, we introduce the invariant loss $\mathcal{L}_{inv}$, according to Proposition 7, will maximize the conditional entropy

$H(\mathbf{s}^{(i)}|\widehat{\mathbf{h}}_G^{(i)})$ for each sample $G^{(i)}$. This encourages the learned representation $\widehat{\mathbf{h}}_G^{(i)}$ to be uninformative about the spurious features $\mathbf{s}^{(i)}$. In the following proof, we drop superscript i for simplicity.

Next, our goal is to show that minimizing $\mathcal{L}$ leads to $\widehat{\mathbf{h}}_G = \mathbf{h}_c$. We consider the following three cases:

Case 1: The encoder learns only spurious features ($\widehat{\mathbf{h}}_G = \mathbf{h}_s$). In this case, the representation $\widehat{\mathbf{h}}_G$ is informative about $\mathbf{s}$ but not about $\mathbf{h}_c$. The conditional entropy $H(\mathbf{s}|\widehat{\mathbf{h}}_G)$ is minimized but not maximized.

Case 2: The encoder learns both invariant and spurious features ($\widehat{\mathbf{h}}_G = \kappa(\mathbf{h}_c, \mathbf{h}_s)$). Here, $\widehat{\mathbf{h}}_G$ is informative about both $\mathbf{h}_c$ and $\mathbf{h}_s$. While this may minimize $\mathcal{L}_{GT}$ in the training environments, $\widehat{\mathbf{h}}_G$ remains informative about $\mathbf{h}_s$, thus not maximizing $H(\mathbf{s}|\widehat{\mathbf{h}}_G)$.

Case 3: The encoder learns only invariant features ($\widehat{\mathbf{h}}_G = \mathbf{h}_c$). In this case, $\widehat{\mathbf{h}}_G$ is uninformative about $\mathbf{h}_s$, therefore, $H(\mathbf{s}|\widehat{\mathbf{h}}_G)$ is greater than previous two cases, furthermore $\widehat{\mathbf{h}}_G$ also minimizes $\mathcal{L}_{GT}$ given the invariant features hold the sufficient predictive power for the targets labels (Assumption 1).

Therefore, we conclude that the encoder $h^*(\cdot)$ will only learn invariant features, as conditioning on spurious features $\mathbf{h}_s$ will not maximize $H(\mathbf{s}|\widehat{\mathbf{h}}_G)$. Additionally, it is important to note that there exists "uninformative" features which may also maximize $H(\mathbf{s}|\widehat{\mathbf{h}}_G)$ without including $\mathbf{h}_c$. This phenomenon has been demonstrated in EQuAD (Yao et al., 2024), where model performance deteriorates when $\lambda > 1$. However, when $\lambda < 1$, $\mathcal{L}_{GT}$ emphasizes useful features that correlate with the target labels, while $\mathcal{L}_{inv}$ acts as a regularization term that encourages the model to remove spurious features and focus on learning invariant features.

□

E COMPLEXITY ANALYSIS

We provide time and space complexity analysis for LIRS, followed by empirical running time analysis on GOODMotif-base and OGBG-Molbbbp datasets.

Space complexity. The space complexity for LIRS is $\mathcal{O}(|\mathcal{B}|Hm)$, where $|\mathcal{B}|$ denotes the batch size, H denotes the hidden feature dimension, and m denotes the average number of edges. Therefore the memory overhead is on par with ERM, and may outperform other graph data augmentation method such as DIR (Wu et al., 2022c) and GREA (Liu et al., 2022), as for each samples, they generate spurious subgraphs for each sample using $|\mathcal{B}|$ samples in the same minibatch, which leads to $\mathcal{O}\left((|\mathcal{B}|^2 + |\mathcal{B}|)Hm\right)$.

Time complexity. The time complexity of LIRS is $\mathcal{O}(kCmF)$, where k is the number of layers in GNN encoder, $C > 1$ is a constant as LIRS runs GNN encoder multiple times, F is the hidden dimension size. Notably, most other graph invariant learning algorithms also exhibit a complexity of $\mathcal{O}(CkmF)$, as they require multiple GNN encoders for subgraph extraction and feature encoding respectively. Therefore, the time cost gap between LIRS and other methods is not significant. We provide a detailed running time analysis using the Motif-base and Ogbg-Molbbbp datasets, as shown in Table 5.

On the Motif-base dataset, the biased infomax only requires 20 epochs training, making its time cost comparable to ERM. On the Ogbg-Molbbbp dataset, the time cost of LIRS exceeds that of other methods since the biased infomax requires training for 100 epochs, and GSAT must be run to annotate node labels to enable adaptive biased infomax. We provide a breakdown of the time cost for each stage in LIRS to provide a better understandings in Table 6.

The first three components account for the majority of the time cost in LIRS, however they only need to be run once. Retraining the GNN encoder is both fast and stable, with less variance as $\mathcal{L}_{Inv}$ is merely a cross-entropy loss. This presents a key advantage of LIRS in terms of hyperparameter selection. Specifically, most of OOD methods require hyperparameter search, and for most methods, the process must be restarted entirely for each run, incurring significant time costs. In contrast, for LIRS, only the final GNN retraining step needs to be run multiple times for hyperparameter

Table 5: Running time analysis (in seconds) on various OOD methods

Method	Motif-base	OGBG-Molbbbp
ERM	494.34±117.86	92.42±0.42
IRM	968.94±164.09	151.84±7.53
Vrex	819.94±124.54	129.13±12.93
GSAT	1233±396.19	142.47±25.71
GREA	1612.43±177.36	262.47±45.71
CIGA	1729.14±355.62	352.14±93.32
AIA	1422.34±69.33	217.36±11.04
OOD-GCL	10813±28.12	8455.51±68.61
EQuAD	747.87±34.71	278.85±16.64
LIRS	504.87±24.04	421.32±19.86

Table 6: Running time analysis (in seconds) of LIRS

Method	Motif-base	OGBG-Molbbbp
Biased Infomax	302.12	214.24
MinibatchKmeans+SVM	6.63	3.04±0.35
Mark Nodes	-	142.47±25.71
GNN Retraining	196.12±24.04	61.57±6.86

search, leading to a significantly reduced time cost when conducting multiple runs compared to other methods.

F More Discussion on LIRS

Comparison with EQuAD (Yao et al., 2024). While LIRS and EQuAD share similarities in the learning paradigm, our study make several distinctions compared with Yao et al. (2024). First, while EQuAD primarily addresses the limitations of existing OOD methods that are sensitive to varying spurious correlation strengths, it does not fully explain why the proposed learning paradigm is effective when spurious correlation strength remains stable. In contrast, our work answer this important question and demonstrates that this learning paradigm enables learning a broader set of invariant features; Second, We curate the *SPMotif-binary* dataset based on the SPMotif datasets, which can serve as a benchmark for future studies to evaluate the effectiveness of methods in learning a broader set of invariant features; Third, While EQuAD uses a standard infomax objective to learn spurious features, we propose a new algorithm that addresses the limitations of the vanilla infomax approach. Specifically, we introduce the biased infomax to overcome size constraints and further incorporate additional procedure (i.e., a GNN explainer) to annotate critical nodes with adaptive thresholding to realize biased infomax in real-world datasets; Finally, We identify the limitations of the cross-entropy loss in disentangling spurious features and propose a novel loss objective that is more effective in learning invariant features. Additionally, our proposed loss does not compromise computational efficiency.

Comparison with Supervised Contrastive Learning (Khosla et al., 2020) and Deep Graph Infomax (Veličković et al., 2018). The biased infomax principle also share similarity with Supervised Contrastive Learning (SCI) and Deep Graph Infomax (DGI). However, SCL and DGI primarily target in-distribution (ID) data and are designed to improve performance on predictive tasks. In contrast, our proposed biased infomax is specifically designed for OOD data, with the goal of learning environment-related features rather than features that directly benefit classification tasks. This makes our approach conceptually distinct from SCL and DGI; Second, In SCL the contrastive loss operates at the inter-sample level, where explicit labels are available for each image. However, in our graph-level OOD setting, biased infomax operates at the node level, where such labels are unavailable. Due to the absence of node labels, we approximate critical nodes using GNN explainer

with adaptive thresholding. This additional procedure also distinct biased infomax from SCL and DGI.

Comparison with OOD-GCL (Li et al., 2024a). LIRS and OOD-GCL both utilize contrastive learning to graph invariant features, however, LIRS relies on labeled data in the subsequent stage to effectively learn invariant features, in contrast, OOD-GCL aims to learn invariant features without labeled data, followed by fine-tuning a linear classifier on downstream tasks. This distinction highlights different assumptions and goals in the design of the two methods. Due to the unavailability of labelled data, OOD-GCL underperforms LIRS across all the datasets. In terms of running time, OOD-GCL is also significantly slower than LIRS and all other methods, as it requires multiple rounds of clustering in every epoch and additional invariance regularization, which must be applied for each channel and cluster.

G Algorithmic Pseudocode

We provide pseudocode for the proposed LIRS framework, which consists of 3 stages for learning spurious features and invariant features respectively. The code will be made publicly available upon acceptance of our work.

H More Details about Experiments

H.1 Datasets Details

Table 7: Details about the datasets used in our experiments.

DATASETS	Split	# TRAINING	# VALIDATION	# TESTING	# CLASSES	METRICS
GOOD-HIV	Scaffold	24682	4113	4108	2	ROC-AUC
	Size	26169	4112	3961	2	ROC-AUC
GOOD-Motif	Base	18000	3000	3000	3	ACC
	Size	18000	3000	3000	3	ACC
OGBG-Molbbbp	Scaffold	1631	204	204	2	ROC-AUC
	Size	1633	203	203	2	ROC-AUC
OGBG-Molbace	Scaffold	1210	152	151	2	ROC-AUC
	Size	1211	151	151	2	ROC-AUC
SPMotif-binary	Correlation	6000	2000	2000	2	ACC
SPMotif($\#G_c = 3$)	Correlation	9000	3000	3000	3	ACC

In this subsection, we provide a detailed introduction to the datasets used in this work, the dataset statistics are illustrated in Table 7.

SPMotif dataset. Following Wu et al. (2022c), we generate a 3-class synthetic datasets based on BAMotif (Ying et al., 2019). In these datasets, each graph comprises a combination of invariant and spurious subgraphs, denoted by G_c and G_s. The spurious subgraphs include three structures (Tree, Ladder, and Wheel), while the invariant subgraphs consist of Cycle, House, and Crane. The task for a model is to determine which one of the three motifs (Cycle, House, and Crane) is present in a graph. A controllable distribution shift can be achieved via a pre-defined parameter b. This parameter manipulates the spurious correlation between the spurious subgraph G_s and the ground-truth label Y, which depends solely on the invariant subgraph G_c. Specifically, given the predefined bias b, the probability of a specific motif (e.g., House) and a specific base graph (Tree) will co-occur is b while for the others is $(1-b)/2$ (e.g., House-Ladder, House-Wheel). When $b = \frac{1}{3}$, the invariant subgraph is equally correlated to the three spurious subgraphs in the dataset. In SPMotif datasets, S is directly influenced by C, and C is causally related with Y. For the variant of the SPMotif datasets used in Section 3, we attach 3 invariant subgraphs G_c to a base spurious subgraph, and in the test dataset, only 1 invariant subgraph is attached to G_s.

SPMotif-binary dataset. To evaluate the feature learning quality of various OOD methods, We curate a binary classification dataset based on the SPMotif dataset, which is utilized in Section 5.3.

Algorithm 1 The LIRS framework

Require: Graph dataset $\mathcal{D}$ with labels $\mathcal{Y}$; training epochs E, E'; threshold τ; hyperparameter γ; regularization weight λ
Ensure: Trained GNN model $f^* = \rho \circ h$
Initialize GNN encoder $h(\cdot)$
for epoch $t = 1$ to E **do** ▷ Step 1: Learning spurious features via biased infomax
  for each graph $G^{(i)}$ in $\mathcal{D}$ **do**
    Obtain graph representation $\mathbf{h}_G^{(i)} \leftarrow h(G^{(i)})$
    Use GNN explainer $e(\cdot)$ to identify important nodes $\widehat{G}_c^{(i)}$
    Remove $\widehat{G}_c^{(i)}$ from $G^{(i)}$ to get $\tilde{G}^{(i)}$
    Compute predicted probabilities $\hat{y}^{(i)} \leftarrow \rho(\mathbf{h}_G^{(i)})$ and $\tilde{y}^{(i)} \leftarrow \rho(h(\tilde{G}^{(i)}))$
    if $|\hat{y}^{(i)} - \tilde{y}^{(i)}| > \tau$ **then**
      Obtain $\mathbf{h}_G^{(i)}$ using Eqn. (2) (biased infomax)
    else
      Obtain $\mathbf{h}_G^{(i)}$ using Eqn. (1) (standard infomax)
    end if
  end for
end for
Obtain spurious embeddings $\{\mathbf{h}_s^{(i)}\}$ from the trained encoder $h(\cdot)$
for each class y in $\mathcal{Y}$ **do** ▷ Step 2: Clustering and Re-fitting Classifier
  Collect spurious embeddings $\{\mathbf{h}_s^{(i)} \mid y^{(i)} = y\}$
  Perform clustering using Minibatch KMeans on $\{\mathbf{h}_s^{(i)}\}$ to get cluster labels $\{c^{(i)}\}$
  Train a linear classifier (e.g., SVM) on $\{\mathbf{h}_s^{(i)}, c^{(i)}\}$ to obtain spurious logits $\mathbf{s}^{(i)}$
end for
Re-initialize GNN encoder $h(\cdot)$, and classification head $\rho(\cdot)$, $\rho'(\cdot)$ ▷ Step 3: Learning invariant features
for epoch $t = 1$ to E' **do**
  for each graph $G^{(i)}$ in $\mathcal{G}$ **do**
    Obtain graph representation $\widehat{\mathbf{h}}_G^{(i)} \leftarrow h(G^{(i)})$
    Compute estimated spurious logits $\widehat{\mathbf{s}}^{(i)} \leftarrow \rho'(\widehat{\mathbf{h}}_G^{(i)})$
    Compute reweighting coefficient $w^{(i)} = \dfrac{1 - (\mathbf{s}_j^{(i)})^\gamma}{\gamma}$, where j is the cluster label
    Compute invariant loss using Eqn. 3
    Update model parameters by minimizing:
      $\mathcal{L} = \mathcal{L}_{\text{ERM}} + \lambda \mathcal{L}_{\text{inv}}$
  end for
end for
return Trained model $f^* = \rho \circ h$

Specifically, the motifs *House* and *Crane* are assigned label 0, and *Diamond* and *Cycle* are assigned label 1. During the construction of each class's samples, we attached both invariant subgraphs to the base subgraph with 50% chance, while in the remaining 50%, we randomly attached one invariant subgraph to the base spurious subgraph. For the test set, we randomly attached a single invariant subgraph to the base subgraph. Similar to the SPMotif dataset, the base spurious subgraph was correlated with the target labels where b controls the correlation strengths, and in the test set an equal correlation strength is assigned for the samples in the same class.

GOOD-HIV is a molecular dataset derived from the MoleculeNet Wu et al. (2018) benchmark, where the primary task is to predict the ability of molecules to inhibit HIV replication. The molecular structures are represented as graphs, with nodes as atoms and edges as chemical bonds. Following Gui et al. (2022), We adopt the covariate shift split, which refers to changes in the input distribution between training and testing datasets while maintaining the same conditional distribution of labels given inputs. This setup ensures that the model must generalize to unseen molecular structures that differ in these domain features from those seen during training. We focus on the Bemis-Murcko

scaffold Bemis & Murcko (1996) and the number of nodes in the molecular graph as two domain features to evaluate our method.

GOOD-Motif is a synthetic dataset designed to test structure shifts. Each graph in this dataset is created by combining a base graph and a motif, with the motif solely determining the label. The base graph type and the size are selected as domain features to introduce covariate shifts. By generating different base graphs such as wheels, trees, or ladders, the dataset challenges the model's ability to generalize to new graph structures not seen during training. We employ the covariate shift split, where these domain features vary between training and testing datasets, reflecting real-world scenarios where underlying graph structures may change.

Open Graph Benchmark. We also use 2 molecule datasets from the graph property prediction task on Open Graph Benchmark Hu et al. (2020) or known as OGBG. They were originally collected by MoleculeNet (Wu et al., 2018) and used to predict the properties of molecules, including (1) blood–brain barrier permeability in MolBBBP; (2) inhibition to human β-secretase 1 in MolBACE. For all molecule datasets, we use the scaffold splitting procedure as OGBG adopted (Hu et al., 2020). It attempts to separate structurally different molecules into different subsets, which provides a more realistic estimate of model performance in experiments (Wu et al., 2018). In addition, we also adopt size split to evaluate the OOD generalization ability for various OOD methods following Sui et al. (2023); Gui et al. (2022).

H.2 Experimental Setup

Encoding spurious features with biased infomax. We adopt MVGRL (Hassani & Khasahmadi, 2020) as the contrastive learning method for learning spurious features. To realize instance-level adaptive biased infomax, we first utilize GSAT (Miao et al., 2022) as the GNN explainability framework to identify important nodes in a graph. The GNN backbone for GSAT is 5-layer GIN (Xu et al., 2018), the hidden dimension is set to 64 for all the datasets except MolHIV, where the hidden dimension is 128. During inference stage, we obtain top-K edges with highest probability in each graph instance and perform counterfactual inference, i.e., after the removal of the subgraph induced by the top-K edges, we record the change in the prediction score Δ_{prob}, and compare with a pre-defined threshold τ to decide whether it should be biased or not. The nodes in a graph will be treated as negative examples during training MVGRL if $\Delta_{prob} > \tau$. In all the experiments, K is searched over: $\{8, 12\}$, τ is searched over: $\{0.2, 0.3\}$. For SPMotif datasets, we directly use the ground-truth nodes from G_c, and don't employ GSAT for approximation.

Generating logits from spurious features and target labels. We use*MiniBatch KMeans* algorithm to obtain the clustering label. To generate (soft) logits as targets from spurious features learned via biased infomax in each cluster, we use linear svm followed by a probability calibrator.

GNN encoder. For SPMotif dataset and SPMotif-binary dataset, we adopt 5-layer GIN (Xu et al., 2018) as backbone GNN encoder with mean pooling; For GOOD-Motif datasets, we utilize a 4-layer GIN with sum pooling, and a hidden dimension of 300; For GOOD-HIV datasets, we employ a 4-layer GIN with sum pooling, and a hidden dimension of 128; For the OGBG-Molbbbp and OGBG-Molbace dataset, we adopt a 4-layer GIN with sum pooling, and the dimensions of hidden layers is 64.

Optimization and evaluation. By default, we use Adam optimizer (Kingma & Ba, 2014) with a learning rate of $1e-3$ and a batch size of 64 for all experiments. we also employ an early stopping of 10 epochs according to the validation performance for all datasets. Test accuracy or ROC-AUC is obtained according to the best validation performance for all experiments. All experiments are run with 4 different random seeds, the mean and standard deviation are reported using the 4 runs of experiments.

Baseline setup and hyperparameters. In our experiments, for the GOOD and OGBG-Molbbbp datasets, the results of ERM, IRM, GroupDRO, and VREx are reported from Gui et al. (2022), while the results for DropEdge, DIR, GSAT, CIGA, GIL, GREA, FLAG, $\mathcal{G}$-Mixup and AIA on GOOD and OGBG datasets are reported from Sui et al. (2023). To ensure fairness, we adopt the same GIN backbone architecture as reported in Sui et al. (2023). For the remaining datasets and methods, we conduct experiments using the provided source codes from the baseline methods. The hyperparameter search is detailed as follows.

For IRM and VREx, the weight of the penalty loss is searched over $\{1e-1, 1, 1e1, 1e2\}$. The causal subgraph ratio for DIR is searched across $\{1e-2, 1e-1, 0.2, 0.4, 0.6\}$. For RSC, the masking ratio is searched over $\{0.2, 0.3, 0.4\}$. For DiverseModel, the number of classifciation headers is searched over $\{5, 10, 20\}$, and the penalty weight of the diversification loss is searched over $\{1e-1, 1e-2, 1e-3\}$. For DropEdge, the edge masking ratio is seached over: $\{0.1, 0.2, 0.3\}$. For GREA, the weight of the penalty loss is tuned over $\{1e-2, 1e-1, 1.0\}$, and the causal subgraph size ratio is tuned over $\{0.05, 0.1, 0.2, 0.3, 0.5\}$. For GIL, the penalty weight is searched over $\{1e-5, 1e-3, 1e-1, 1.0\}$, and the number of environments is searched over $\{3, 5, 10\}$. For GSAT, the causal graph size ratio is searched over $\{0.3, 0.5, 0.7\}$. For CIGA, the contrastive loss hinge loss weights are searched over $\{0.5, 1.0, 2.0, 4.0, 8.0\}$. For DisC, we search over q in the GCE loss: $\{0.5, 0.7, 0.9\}$. For LiSA, the loss penalty weights are searched over:$\{1, 1e-1, 1e-2, 1e-3\}$. For FLAG, the ascending steps are set to 3 as recommended in the paper, and the step size is searched over $\{1e{-}3, 1e{-}2, 1e{-}1\}$. For AIA, the stable feature ratio is searched over $\{0.1, 0.3, 0.5, 0.7, 0.9\}$, and the adversarial penalty weight is searched over $\{0.01, 0.1, 0.2, 0.5, 1.0, 3.0, 5.0\}$. For EQuAD, the penalty weight is searched over $\{1e-1, 1e-2, 1e-3\}$, and the reweighting coefficient is searched over $\{0.1, 0.3, 0.5, 0.7, 0.9\}$.

Hyperparameter search for LIRS. The penalty weight for $\mathcal{L}_{\text{Inv}}$ in LIRS is searched over $\{1e-1, 1e{-}2, 1e{-}3\}$. The reweighting coefficient γ is searched over $\{0.1, 0.3, 0.5, 0.7, 0.9\}$. The cluster number C is searched over $\{3, 5, 10\}$. The training epoch E at which the spurious embedding is derived from the biased infomax is searched over $\{50, 60, 70, 80, 90\}$ for real-world datasets, and for the synthetic datasets, The training epoch E is searched over $\{5, 6, 7, 8, 9\}$.

Implementation of LIRS. We extend the code from GSAT (Miao et al., 2022) to annotate the nodes in each graph to be biased in real-world datasets. We adopt PyGCL (Zhu et al., 2021) package and modify the source code in *DualBranchContrast* to implement the biased infomax to generate spurious embeddings. To generate logits from the spurious embeddings, we use *MiniBatchKMeans*, *linearSVC*, and *CalibratedClassifierCV* in Scikit-Learn package (Pedregosa et al., 2011). We use PyTorch Paszke et al. (2019) and Pytorch-Geometric Fey & Lenssen (2019) for the remaining implementation.

H.3 Additional Experimental Results

Visualization of latent features derived from the biased infomax. We provide visualization of the 2d latent embedding derived form the biased infomax. Specifically, we utilize the SPMotif datasets and GOODMotif datasets to assess the correlation between the learned embeddings after dimensionality reduction and environment labels within each class. We annotate each data sample with the environment label corresponding to three spurious patterns (Tree, Ladder, and Wheel). We then use the spurious features obtained from the biased infomax objective, apply t-SNE Van der Maaten & Hinton (2008) for dimensionality reduction, and use KMeans for clustering and visualization. The epoch at which the latent embedding is obtained is selected according to the best hyperparameter. In Figure 6, points of different colors correspond to different environment labels. It can be observed that within each class, the clusters highly correlate with environments, indicating that the biased infomax effectively captures different spurious patterns.

H.4 Software and hardware

All the experiments are ran with PyTorch (Paszke et al., 2019) and PyTorch Geometric (Fey & Lenssen, 2019). We run all the experiments on Linux servers with RTX 4090 and CUDA 12.2.

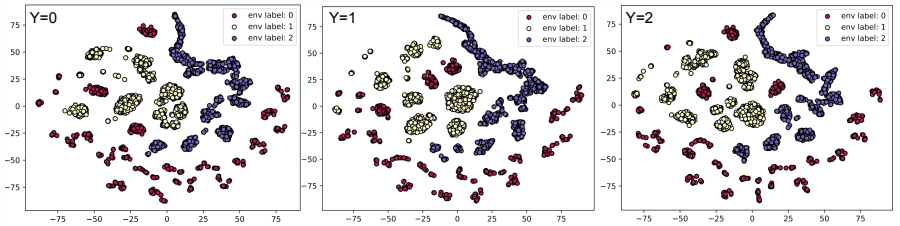

(a) GOODMotif-base

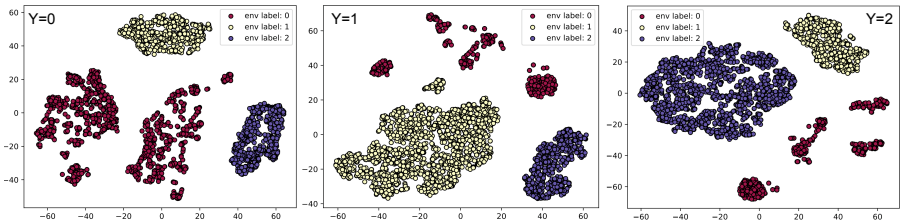

(b) SPMotif-0.60 ($\#G_c = 3$)

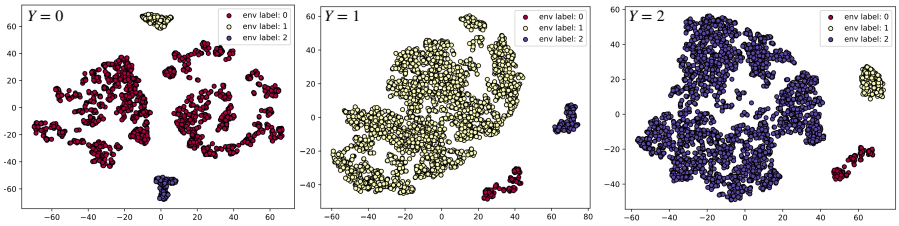

(c) SPMotif-0.90 ($\#G_c = 3$)

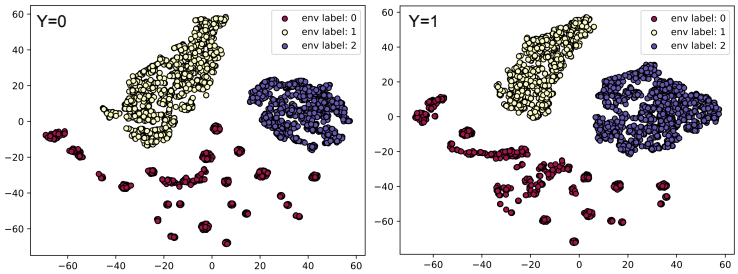

(d) SPMotif-binary-0.40

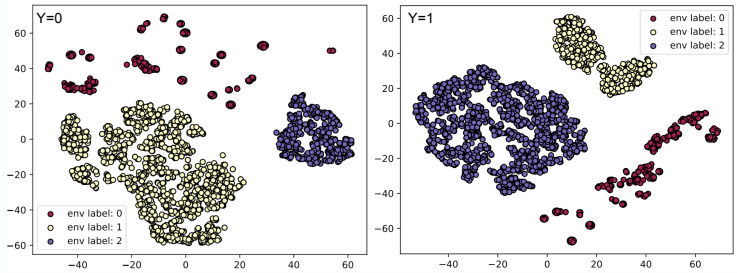

(e) SPMotif-binary-0.60

Figure 6: Clustering visualizations using latent embeddings derived from the biased infomax. The clusters resulted from latent embeddings obtained from the biased infomax are highly correlated with the environment labels.